On high order methods for the heterogeneous Helmholtz equation

Théophile Chaumont-Frelet

ON HIGH ORDER METHODS FOR THE HETEROGENEOUS HELMHOLTZ EQUATION

THÉOPHILE CHAUMONT-FRELET

Abstract. The heterogeneous Helmholtz equation is used in Geophysics to model the propagation of a time harmonic wave through the Earth. Processing seismic data (inversion, migration...) involves many solutions of the Helmholtz equation, so that an efficient numerical algorithm is required. It turns out that obtaining numerical approximations of waves becomes very demanding at high frequencies because of the pollution effect. In the case of homogeneous media, high order methods can reduce the pollution effect significantly, enabling the approximation of high frequency waves. However, they fail to handle fine-scale heterogeneities and can not be directly applied to heterogeneous media. In this paper, we show that if the propagation medium is properly approximated using a multiscale strategy, high order methods are able to capture subcell variations of the medium. Furthermore, focusing on a one-dimensional model problem enables us to prove frequency explicit asymptotic error estimates, showing the superiority of high order methods. Numerical experiments validate our approach and comfort our theoretical results.

Introduction

Numerical approximation of high frequency waves is a challenging problem: because of the pollution effect, meshes need to be drastically refined. In the context of Galerkin methods, the pollution effect is the fact that if the number of degrees of freedom per wavelength is fixed, the error of the best approximation of the discrete space remains bounded, while the numerical solution is diverging from the true solution when the frequency is increasing. This is due to the fact that the Helmholtz operator is not coercive, so that quasi-optimality of the discrete scheme is not ensured for arbitrary meshes.

The pollution effect has been extensively studied in the case of homogeneous media. In particular, it is known that even if it is possible to design pollution-free schemes in one dimension, it is not the case in two and three dimensions, as shown by Babuška and Sauter in [11].

Frequency explicit error estimates have been derived: the finite element error is bounded explicitly in terms of the frequency ω, the mesh step h and the order of discretization p. Two types of results are available. First, if the mesh is fine enough, the finite element

Key words and phrases. Wave propagation; Helmholtz equation; Heterogeneous media; Pollution effect; High order methods; Multiscale methods .

This work was partially supported by the project M2NUM (M2NUM is co-financed by the European Union with the European regional development fund (ERDF, HN0002137) and by the Normandie Regional Council) and the INRIA-TOTAL strategic action DIP (`http://dip.inria.fr`).

solution is quasi-optimal. These results are called asymptotic error estimates. The second type of results are the so-called pre-asymptotic error estimates. They give an optimal condition on the mesh to bound the error independently of the frequency.

For the case of one-dimensional homogeneous media, optimal pre-asymptotic error estimates for Lagrangian polynomial discretizations have been established by Babuška and Ihlenburg in the pair of papers [5, 6]. It is shown that the error can be decomposed into two different terms. The best approximation error, of order $\omega^p h^p$, and the phase lag, of order $\omega^{2p+1}h^{2p}$. In particular, the error is bounded independently of the frequency, if $h \simeq \omega^{-1-1/(2p)}$. The pollution effect is present for all p, since the mesh step must satisfy $h \simeq \omega^{-1-1/(2p)} << \omega^{-1}$. However, this effect is reduced for high order methods, since the exponent on ω rapidly approaches one as p increases.

Asymptotic error estimates are available in two and three dimensions. Melenk and Sauter showed in [8, 9] that finite element schemes are stable and that the finite element solution is quasi-optimal under the condition that $\omega^{p+1}h^p < C$.

In this paper, we focus on the case of highly heterogeneous media. Classical high order discretizations often fail to handle such propagation media, because they are unable to see the fine scales of the velocity parameter. Indeed, they are usually built using coarser meshes than low order methods. Therefore, if the velocity parameter is selected to be constant in each cell (through averaging, or local homogenization strategies), fine scale information is (at least partially) lost. Furthermore, restricting the mesh step so that the velocity parameter is constant inside each cell usually increases the computational cost drastically if the medium is highly heterogeneous.

We propose to overcome this difficulty with a Multiscale Medium Approximation method (MMAm). The velocity parameter is not assumed to be constant on each cell, but on a submesh of each cell. If the submeshes are properly designed, the MMAm is equivalent to a quadrature formula adapted to the medium. In particular, we show that this methodology has roughly the same computational cost as the classical finite element method. The method was presented in [1] for a two-dimensional Helmholtz problem, and a pre-asymptotic error estimate has been demonstrated for linear elements.

The key aspect of the MMAm is its ability to handle jumps of the velocity parameter inside the mesh cells. As a result, the MMAm enables the user to select larger mesh steps than the characteristic length of the heterogeneities, which drastically reduces the computational cost in highly heterogeneous media.

The aim of this paper is to extend the analysis of the MMAm presented in [1] for linear elements to higher order discretizations. Though practical applications are 3D, we focus on a one-dimensional model problem. This choice enables us to simplify the proofs, but we believe that our results carry over two-dimensional and three-dimensional problems in layered media.

First, we show that the heterogeneous Helmholtz problem is well-posed and derive frequency explicit stability estimates with respect to the right hand side, and with respect to variations of the velocity parameter, justifying the use of medium approximation. Those

results are obtained assuming that the velocity parameter is monotone and that the propagation medium is surrounded by first order absorbing boundary conditions. However, these hypothesis are not mandatory to discretize the problem.

Second, we derive asymptotic error estimates for the MMAm. Even if the solution can be rough inside each cell because of velocity jumps, we are able to extend the asymptotic error estimates obtained in [8] for $1 \leq p \leq 3$.

Third, we investigate numerically the stability of the scheme when the frequency is increasing to determine optimal meshing conditions. We show that in simple media, the optimal pre-asymptotic error estimates derived in homogeneous media are still valid. However, when considering more complex cases, it looks like the condition $h \simeq \omega^{-1-1/(2p)}$ is insufficient.

Finally, we fix the frequency and compare different orders of discretization to achieve a given accuracy. We are able to conclude that high order methods provide superior approximations: in our examples, $p = 4$ discretizations always yield a smaller linear system than lower order discretizations for the same accuracy.

The paper is organized as follow: in Section 1, we define our model problem and introduce the notations. Section 2 is devoted to the analysis of the continuous problem. We analyse the MMAm in Section 3, 4 and 5 and numerical experiments are presented in Sections 6 and 7.

1. Settings

We consider the Helmholtz equation set in the heterogeneous one-dimensional domain $(0, Z)$ with absorbing boundary conditions

$$\left\{\begin{array}{rcl} -\dfrac{\omega^2}{c^2(z)}u(z) - u''(z) &=& f(z), \quad z \in (0, Z), \\ -u'(0) - \dfrac{\mathbf{i}\omega}{c(0)}u(0) &=& 0, \\ u'(Z) - \dfrac{\mathbf{i}\omega}{c(Z)}u(Z) &=& 0, \end{array}\right. \tag{1}$$

where f is the load term, ω is the pulsation and c is the velocity parameter. Since we especially focus on the high frequency case, we will consider real frequencies $\omega \geq 1$.

For the sake of simplicity, we restrict ourselves to the case where c is piecewise constant. We could also have considered piecewise smooth velocity parameters. We do not because we consider that the most difficult part of the analysis is the jumps of the parameter, which are considered herein. We will also assume that all the velocity parameters we consider are uniformly bounded above and below by two constants. This is a reasonable assumption, which can be justified in geophysics by the properties of rocks. We also introduce two additional hypothesis which are required for our theoretical analysis. We will assume that the length of the thinest layer is bounded below and that the velocity parameter is monotone. Remark that the monotonicity hypothesis is still valid in a lot of geophysical

applications, since the wavespeed is usually increasing with depth. Our assumptions on c are summarized in Definition 1.

Definition 1. *We consider parameters c which are piecewise constant and non-increasing. Let $0 = z_0 < z_1 < \cdots < z_{L-1} < z_L = Z$, then we will note*

$$c|_{(z_{l-1},z_l)} = c_l \in \mathbb{R},$$

such that $c_l < c_{l-1}$. We will also note

$$\left[\frac{1}{c^2}\right]_l = \frac{1}{c_l^2} - \frac{1}{c_{l-1}^2} > 0.$$

Furthermore, we assume that $c_L = c_{max}$, $c_1 = c_{min}$ and $\min_l z_l - z_{l-1} > \nu$, where $\nu > 0$ is the thinest acceptable layer length and $0 < c_{min} < c_{max}$ are the minimal and maximal possible velocities.

Remark that since the size of each layer is bounded below by ν, there is a maximum number of layers that can be considered. More precisely, we have $L < Z/\nu$.

In the remaining of this paper, we use the following notations. $L^2(0,Z)$ denotes the space of square-integrable complex-valued functions on $(0,Z)$. If $v \in L^2(0,Z)$, we denote

$$||v|| = \left(\int_0^Z |v(z)|^2 dz\right)^{1/2}$$

the norm of v. $H^k(0,Z)$ is the standard Sobolev space of order k. If $v \in H^1(0,Z)$, we note $v' \in L^2(0,Z)$ its derivative in the sense of distribution. We denote by $L^\infty(0,Z)$ the space of essentially bounded functions and for $v \in L^\infty(0,Z)$, we note

$$||v||_\infty = \text{esssup}_{(0,Z)} |v|.$$

$L^1(0,Z)$ is the space of integrable functions. For $v \in L^1(0,Z)$, we note

$$||v||_1 = \int_0^Z |v(z)| dz$$

its norm.

We also introduce, for $v \in H^1(0,Z)$, the (ω and c dependant) norm

$$||v||_{\omega,c}^2 = \omega^2 ||c^{-1}v||^2 + ||v'||^2.$$

For the sake of simplicity, we now assume that $f \in L^2(0,Z)$. Then, it is well known that $u \in H^1(0,Z)$ is solution to (1) in a weak sense iff

$$B_{\omega,c}(u,v) = \int_0^Z f(z)\overline{v(z)}dz, \quad \forall v \in H^1(0,Z), \tag{2}$$

where

$$B_{\omega,c}(u,v) = -\omega^2 \int_0^Z \frac{1}{c^2(z)} u(z)\overline{v(z)}dz - \frac{\mathbf{i}\omega}{c_{max}} u(0)\overline{v(0)} - \frac{\mathbf{i}\omega}{c_{min}} u(Z)\overline{v(Z)} + \int_0^Z u'(z)\overline{v'(z)}dz. \tag{3}$$

2. Analysis of the continuous problem

To the best of our knowledge, the first stability result for the Helmholtz equation is given by Douglas et Al. in [3]. The analysis is limited to the one-dimensional homogeneous problem and uses the explicit expression of the Green's function. A similar approach is used by Ihlenburg and Babuška in [5]. In the case of two-dimensional bounded domains surrounded by absorbing boundary conditions, the explicit expression of the Green's function is not available, and other methodologies must be used. A stability proof has been developed for star-shaped two-dimensional domains by Melenk [7] using the test function $v(x) = x \cdot \nabla u(x)$ and integral identities. This proof was extended to three-dimensional domains and mixed boundary conditions by Hetmaniuk [4].

In [1], we showed that the method used by Melenk and Hetmaniuk [7, 4] can be extended to two-dimensional star-shaped domains with piecewise-constant velocity satisfying a monotonicity assumption. Actually, the same test function and integration by parts techniques can be used. However, additional terms appears because of the variations of c. The key idea of the proof is that these terms can be omitted if the monotone hypothesis is satisfied.

In this paper, we focus on a simpler one-dimensional problem. It permits to bound the norm of the solution by the norm of the right hand side with a simpler constant than in the two-dimensional case. We also bound the value of the solution at the interfaces of the medium. This property will become important in the error analysis of the MMAm.

We also retrieve the shape of the problem Green's function up to complex constants. If the frequency is high enough, we are able to bound those constants and derive a sharp stability estimate in L^∞ norm.

We mention that some of the results of this section can be extended to two-dimensional and probably three-dimensional media. In particular, two-dimensional versions of Theorem 1, Corollary 1, Proposition 2 and Theorem 2 are proved in [1] under a similar assumption on the velocity parameter. However, the proof of Proposition 1 is strongly linked to the fact that we are considering a one-dimensional problem.

We start our analysis with a stability result for problem (2) presented in Theorem 1, hence deducing the well-posedness (Corollary 1) using the Fredholm alternative. We then turn to sharp stability estimates of the L^∞ norm of the solution's derivative at high frequencies. In the end of the section, we show that problem (2) is stable under perturbation of the velocity parameter c. The proof of Theorem 1 is carried out as an adaptation of [4].

Theorem 1. *Let $u \in H^1(0, Z)$ be any solution to (2). Then u satisfies*

$$\omega^2 ||c^{-1}u||^2 + ||u'||^2 + 2\omega^2 \sum_{l=1}^{L-1} \left[\frac{1}{c^2}\right]_l z_l |u(z_l)|^2 \leq C_s^2 ||f||^2,$$

with

$$C_s = 2\frac{Z c_{max}}{c_{min}}.$$

Proof. As a starting point, we pick $v = zu'$ as a test function in (2). Using identities (39) and (40) derived in the appendix, we have

$$2\text{Re } B_{\omega,c}(u, zu') = \omega^2 \int_0^Z \frac{1}{c(z)^2}|u(z)|^2 dz + \omega^2 \sum_{l=1}^{L-1} \left[\frac{1}{c^2}\right] z_l |u(z_l)|^2 + \int_0^Z |u'(z)|^2 dz + Z|u'(Z)|^2 - \frac{\omega^2 Z|u(Z)|^2}{c_{min}^2} - 2\text{Re } \mathbf{i}\frac{\omega Z}{c_{min}} u(Z)\overline{u'(Z)},$$

so that

$$\omega^2||c^{-1}u||^2 + ||u'||^2 + \omega^2 \sum_{l=1}^{L-1} \left[\frac{1}{c^2}\right] z_l|u(z_l)|^2 + Z|u'(Z)|^2 = 2\text{Re } \int_0^Z f(z)z\overline{u'(z)}dz + \frac{\omega^2 Z|u(Z)|^2}{c_{min}^2} + 2\text{Re } \mathbf{i}\frac{\omega Z}{c_{min}} u(Z)\overline{u'(Z)}. \tag{4}$$

We need to upper bound the right hand side of (4). We proceed the following way

$$\begin{aligned} 2\text{Re } \int_0^Z f(z)z\overline{u'(z)}dz &\leq 2Z||f||||u'|| \leq 2Z^2||f||^2 + \frac{1}{2}||u'||^2, \\ 2\text{Re } \mathbf{i}\frac{\omega Z}{c_{min}} u(Z)\overline{u'(Z)} &\leq 2\frac{\omega Z}{c_{min}}|u(Z)||u'(Z)| \leq \frac{\omega^2 Z}{c_{min}^2}|u(Z)|^2 + Z|u'(Z)|^2, \end{aligned}$$

and we obtain

$$\omega^2||c^{-1}u||^2 + \frac{1}{2}||u'||^2 + \omega^2 \sum_{l=1}^{L-1} \left[\frac{1}{c^2}\right] z_l|u(z_l)|^2 \leq 2Z^2||f||^2 + \frac{\omega^2 Z}{c_{min}^2}|u(Z)|^2. \tag{5}$$

To conclude the proof, we need to bound the last term in the right hand side of (5). We pick $v = u$ as a test function in (2), so that

$$-\frac{\omega}{c_{max}}|u(0)|^2 - \frac{\omega}{c_{min}}|u(Z)|^2 = \text{Im } \int_0^Z f(z)\overline{u(z)}dz,$$

and

$$\frac{\omega}{c_{min}}|u(Z)|^2 \leq ||cf||||c^{-1}u||.$$

We complete the demonstration with

$$\begin{aligned} \frac{\omega^2 Z}{c_{min}^2}|u(Z)|^2 &\leq \frac{\omega Z}{c_{min}}||cf||||c^{-1}u|| \\ &\leq \frac{Z^2}{2c_{min}^2}||cf||^2 + \frac{\omega^2}{2}||c^{-1}u||^2 \\ &\leq \frac{Z^2 c_{max}^2}{2c_{min}^2}||f||^2 + \frac{\omega^2}{2}||c^{-1}u||^2. \end{aligned}$$

We then obtain

$$\frac{\omega^2}{2}||c^{-1}u||^2 + \frac{1}{2}||u'||^2 + \omega^2 \sum_{l=1}^{L-1} \left[\frac{1}{c^2}\right]_l z_l |u(z_l)|^2 \leq Z^2 \left(2 + \frac{1}{2}\frac{c_{max}^2}{c_{min}^2}\right) ||f||^2,$$

and

$$\omega^2||c^{-1}u||^2 + ||u'||^2 + 2\omega^2 \sum_{l=1}^{L-1} \left[\frac{1}{c^2}\right]_l z_l |u(z_l)|^2 \leq 4 \left(\frac{Z c_{max}}{c_{min}}\right)^2 ||f||^2.$$

□

In the next corollary, we use the Fredholm alternative to show that problem (2) admits a unique solution. This way, we are able to introduce the solution operator $\mathcal{S}_{\omega,c}$ and to derive various stability estimates.

Corollary 1. *For all $f \in L^2(0, Z)$, there exists a unique $\mathcal{S}_{\omega,c} f \in H^1(0, Z)$, such that*

$$B_{\omega,c}(\mathcal{S}_{\omega,c} f, v) = \int_0^Z f(z)\overline{v(z)}dz,$$

and the following estimates hold

$$||\mathcal{S}_{\omega,c} f||_{\omega,c} \leq C_s ||f|| \tag{6}$$

$$\omega \sum_{l=1}^{L-1} \left[\frac{1}{c^2}\right]_l |(\mathcal{S}_{\omega,c} f)(z_l)| \leq C_{s,j} ||f||, \tag{7}$$

where

$$C_{s,j} = \frac{c_{max} c_{min}}{\sqrt{2\nu}\sqrt{c_{max}^2 - c_{min}^2}} C_s.$$

Furthermore, $\mathcal{S}_{\omega,c} f \in H^2(0, Z)$ and

$$||(\mathcal{S}_{\omega,c} f)''|| \leq C_{s,2}\omega ||f||, \tag{8}$$

with

$$C_{s,2} = 1 + c_{max} C_s.$$

Proof. First, observe that the sesquilinear form B satisfies a Gårding inequality. Indeed, for all $v \in H^1(0, Z)$, we have

$$\text{Re } B_{\omega,c}(v, v) = -\omega^2||c^{-1}v||^2 + ||v'||^2 \geq ||v'||^2 - \frac{\omega^2}{c_{min}^2}||v||^2.$$

Therefore, the existence of $\mathcal{S}_{\omega,c} f$ follows from uniqueness. But Theorem 1 with $f = 0$ implies uniqueness, and existence and uniqueness of $\mathcal{S}_{\omega,c} f$ are proved.

It is clear that estimate (6) is a direct consequence of Theorem 1. For estimate (7), Theorem 1 yields

$$\omega^2 \sum_{l=1}^{L-1} \left[\frac{1}{c^2}\right]_l z_l |(\mathcal{S}_{\omega,c} f)(z_l)|^2 \leq \frac{C_s^2}{2} ||f||^2.$$

Since $z_l > z_1 > \nu$, we can derive

$$\omega^2 \sum_{l=1}^{L-1} \left[\frac{1}{c^2}\right]_l |(\mathcal{S}_{\omega,c} f)(z_l)|^2 \leq \frac{C_s^2}{2\nu} ||f||^2,$$

and we conclude using the Cauchy-Schwarz inequality

$$\begin{aligned} \omega \sum_{l=1}^{L-1} \left[\frac{1}{c^2}\right]_l |(\mathcal{S}_{\omega,c} f)(z_l)| &= \omega \sum_{l=1}^{L-1} \left[\frac{1}{c^2}\right]_l^{1/2} \left[\frac{1}{c^2}\right]_l^{1/2} |(\mathcal{S}_{\omega,c} f)(z_l)| \\ &\leq \left(\sum_{l=1}^{L-1} \left[\frac{1}{c^2}\right]_l\right)^{1/2} \left(\omega^2 \sum_{l=1}^{L-1} \left[\frac{1}{c^2}\right]_l |(\mathcal{S}_{\omega,c} f)(z_l)|^2\right)^{1/2}, \end{aligned}$$

together with

$$\left(\sum_{l=1}^{L-1} \left[\frac{1}{c^2}\right]_l\right)^{1/2} = \left(\frac{1}{c_{min}^2} - \frac{1}{c_{max}^2}\right)^{1/2} = \frac{\sqrt{c_{max}^2 - c_{min}^2}}{c_{max} c_{min}}.$$

We now turn to the last part of the corollary. Since $\mathcal{S}_{\omega,c} f$ is weak solution to (1), we have

$$(\mathcal{S}_{\omega,c} f)'' = -f - \omega^2 \mathcal{S}_{\omega,c} f.$$

In particular, it follows that $(\mathcal{S}_{\omega,c} f)'' \in L^2(0, Z)$ and $\mathcal{S}_{\omega,c} f \in H^2(0, Z)$. We now prove estimate (8):

$$\begin{aligned} ||(\mathcal{S}_{\omega,c} f)''|| &\leq ||f|| + \omega^2 ||\mathcal{S}_{\omega,c} f|| \\ &\leq ||f|| + \omega c_{max} ||\mathcal{S}_{\omega,c} f||_{\omega,c} \\ &\leq (1 + C_s c_{max} \omega) ||f|| \\ &\leq (C_s c_{max} + 1) \omega ||f||. \end{aligned}$$

□

We now turn to the proof of a sharp estimate of the solution's derivative in L^∞ norm. Indeed, this result is crucial for the upcoming finite element error analysis. An additional hypothesis is required. From now on, we assume that

$$\omega \geq \max_{l \in \{1,\dots,L\}} \left\{\frac{2c_l}{z_l - z_{l-1}}\right\}. \tag{9}$$

In order to derive estimate (12), we need the explicit form of the solution. In Lemma 1, we retrieve the shape of the solution up to complex constants using ODE theory. Furthermore, we are able to bound the constants under the condition that the frequency is high enough.

Lemma 1. *Consider $f \in L^2(0, Z)$. In each interval (z_{l-1}, z_l), we have*

$$(\mathcal{S}_{\omega,c} f)(z) = \alpha_l \exp\left(\frac{\mathbf{i}\omega}{c_l} z\right) + \beta_l \exp\left(-\frac{\mathbf{i}\omega}{c_l} z\right) + \frac{\mathbf{i} c_l}{2\omega} \int_0^Z f(\xi) \exp\left(\frac{\mathbf{i}\omega}{c_l} |z - \xi|\right) d\xi, \tag{10}$$

for two constants $\alpha_l, \beta_l \in \mathbb{C}$ *and a.e* $z \in (z_{l-1}, z_l)$*. Furthermore, there holds*

$$|\alpha_l|^2 + |\beta_l|^2 \leq \frac{C_{\alpha,\beta}^2}{\omega^2}||f||^2, \tag{11}$$

with

$$C_{\alpha,\beta} = \sqrt{\frac{2}{\nu}}\left(C_s + \frac{Z}{2}\right) c_{max}.$$

Proof. To start with, expression (10) is due to the fact that on each interval (z_{l-1}, z_l), $\mathcal{S}_{\omega,c}f$ is solution to the following ODE

$$-\frac{\omega^2}{c_l^2}\mathcal{S}_{\omega,c}f - (\mathcal{S}_{\omega,c}f)'' = f.$$

The key item is now to use Theorem 1 to bound α_l and β_l. Condition (9) that ω is high enough will be used. Because of (10), we have

$$\begin{aligned}\left|\left|\left[\alpha_l \exp\left(\frac{\mathbf{i}\omega}{c_l}z\right) + \beta_l \exp\left(-\frac{\mathbf{i}\omega}{c_l}z\right)\right]\mathbf{1}_{(z_{l-1},z_l)}\right|\right| &\leq ||(\mathcal{S}_{\omega,c}f)\mathbf{1}_{(z_{l-1},z_l)}|| \\ &+ \frac{c_l}{2\omega}\left|\left|\left[\int_0^Z f(\xi)\exp\left(\frac{\mathbf{i}\omega}{c_l}|z-\xi|\right)d\xi\right]\mathbf{1}_{(z_{l-1},z_l)}\right|\right|\end{aligned}$$

We can bound the right hand side. We have

$$\left|\left|\left[\int_0^Z f(\xi)\exp\left(\frac{\mathbf{i}\omega}{c_l}|z-\xi|\right)d\xi\right]\mathbf{1}_{(z_{l-1},z_l)}\right|\right| \leq \left|\left|\int_0^Z |f(\xi)|d\xi\right|\right| = \sqrt{Z}\int_0^Z |f(\xi)|d\xi \leq Z||f||,$$

and $||(\mathcal{S}_{\omega,c}f)\mathbf{1}_{(z_{l-1},z_l)}|| \leq ||\mathcal{S}_{\omega,c}f|| \leq C_s c_{max}\omega^{-1}||f||$ by (6). It follows that

$$\left|\left|\left[\alpha_l \exp\left(\frac{\mathbf{i}\omega}{c_l}z\right) + \beta_l \exp\left(-\frac{\mathbf{i}\omega}{c_l}z\right)\right]\mathbf{1}_{(z_{l-1},z_l)}\right|\right| \leq \left(C_s c_{max} + \frac{Zc_l}{2}\right)\frac{1}{\omega}||f||.$$

We now give a lower bound of the left hand side, assuming that ω is high enough. We have

$$\left|\alpha_l \exp\left(\frac{\mathbf{i}\omega}{c_l}z\right) + \beta_l \exp\left(-\frac{\mathbf{i}\omega}{c_l}z\right)\right|^2 = |\alpha_l|^2 + |\beta_l|^2 + 2\text{Re }\alpha_l\overline{\beta_l}\exp\left(\frac{2\mathbf{i}\omega}{c_l}z\right)$$

so that

$$\begin{aligned}\left|\left|\left[\alpha_l \exp\left(\frac{\mathbf{i}\omega}{c_l}z\right)+\beta_l\exp\left(-\frac{\mathbf{i}\omega}{c_l}z\right)\right]\mathbf{1}_{(z_{l-1},z_l)}\right|\right|^2 &= (z_l-z_{l-1})(|\alpha_l|^2+|\beta_l|^2)\\ &+ 2\mathrm{Re}\ \alpha_l\overline{\beta_l}\int_{z_{l-1}}^{z_l}\exp\left(\frac{2\mathbf{i}\omega}{c_l}z\right)dz\\ &= (z_l-z_{l-1})(|\alpha_l|^2+|\beta_l|^2)\\ &+ 2\mathrm{Re}\ \alpha_l\overline{\beta_l}\frac{c_l}{2\mathbf{i}\omega}\left[\exp\left(\frac{2\mathbf{i}\omega}{c_l}z\right)\right]_{z_{l-1}}^{z_l}\\ &\geq (z_l-z_{l-1})(|\alpha_l|^2+|\beta_l|^2)-\frac{2c_l}{\omega}|\alpha_l||\beta_l|.\\ &\geq \left((z_l-z_{l-1})-\frac{c_l}{\omega}\right)(|\alpha_l|^2+|\beta_l|^2).\end{aligned}$$

Using (9), we obtain

$$|\alpha_l|^2+|\beta_l|^2\leq\frac{2}{z_l-z_{l-1}}\left(C_s c_{max}+\frac{Zc_l}{2}\right)^2\frac{1}{\omega^2}||f||^2,$$

and the result follows. □

We are now able to provide a sharp bound to the solution's derivative at high frequencies (i.e. assuming that (9) holds). Proposition 1 will play an important role in the analysis of finite element discretizations.

Proposition 1. *There holds*

$$||(\mathcal{S}_{\omega,c}f)'||_\infty\leq C_\infty||f||, \tag{12}$$

where

$$C_\infty=\frac{2}{C_{\alpha,\beta}c_{min}}+\frac{\sqrt{Z}}{2}.$$

Proof. Consider a single interval (z_{l-1},z_l). Recalling expression (10), we have

$$(\mathcal{S}_{\omega,c}f)'(z)=\frac{\mathbf{i}\omega\alpha_l}{c_l}\exp\left(\frac{\mathbf{i}\omega}{c_l}z\right)-\frac{\mathbf{i}\omega\beta_l}{c_l}\exp\left(-\frac{\mathbf{i}\omega}{c_l}z\right)-\frac{1}{2}\int_0^Z f(\xi)\,\mathrm{Sgn}(z-\xi)\exp\left(\frac{\mathbf{i}\omega}{c_l}|z-\xi|\right)d\xi,$$

and therefore

$$|(\mathcal{S}_{\omega,c}f)'(z)|\leq\frac{\omega}{c_l}|\alpha_l|+\frac{\omega}{c_l}|\beta_l|+\frac{1}{2}\int_0^Z|f(\xi)|d\xi,$$

for all $z\in(z_{l-1}-z_l)$. Therefore, according to (11) it is clear that

$$|(\mathcal{S}_{\omega,c}f)'(z)|\leq\frac{2C_{\alpha,\beta}}{c_l}||f||+\frac{\sqrt{Z}}{2}||f||\leq\left(\frac{2C_{\alpha,\beta}}{c_{min}}+\frac{\sqrt{Z}}{2}\right)||f||, \tag{13}$$

and (12) follows, since (13) holds for almost every $z\in(0,Z)$. □

In Proposition 2 we define the adjoint operator $\mathcal{S}^\star_{\omega,c}$. The adjoint operator will be used to derive inf-sup conditions on the continuous and discrete level.

Proposition 2. *For all $f \in L^2(0,Z)$, we define $\mathcal{S}^\star_{\omega,c} f = \overline{\mathcal{S}_{\omega,c}\bar{f}} \in H^1(0,Z)$. Then we have*

$$B_{\omega,c}(v, \mathcal{S}^\star_{\omega,c} f) = \int_0^Z v(z)\overline{f(z)}dz,$$

for all $v \in H^1(0,Z)$. Furthermore, we have

$$||\mathcal{S}^\star_{\omega,c} f||_{\omega,c} \leq C_s ||f||. \tag{14}$$

Proof. The proof is very simple. Indeed, considering an arbitrary $v \in H^1(0,Z)$, we have

$$B_{\omega,c}(v, \mathcal{S}^\star_{\omega,c} f) = B_{\omega,c}(\overline{\mathcal{S}^\star_{\omega,c} f}, \bar{v}) = B_{\omega,c}(S_{\omega,c}\bar{f}, \bar{v}) = \int_0^Z \overline{f(z)} v(z) dz.$$

Estimate (14) is a direct consequence of (6). □

In Theorem 2, we use proposition 2 to show that the sesquilinear form B satisfies an inf-sup condition. Our proof is based on the same arguments than Ihlenburg and Babuška [5].

Theorem 2. *We have*

$$\inf_{u \in H^1(0,Z)} \sup_{v \in H^1(0,Z)} \frac{Re\ B_{\omega,c}(u,v)}{||u||_{\omega,c}||v||_{\omega,c}} \geq \frac{C_\gamma}{\omega}, \tag{15}$$

with

$$C_\gamma = \frac{c_{min}}{c_{min} + 2C_s}.$$

Proof. Consider an arbitrary $u \in H^1(0,Z)$. We define

$$s^\star = 2\mathcal{S}^\star_{\omega,c}\left(\frac{\omega^2}{c^2}u\right),$$

so that, by proposition 2, we have

$$\text{Re } B_{\omega,c}(u, u + s^\star) = ||u||^2_{\omega,c}.$$

We conclude the proof with (14):

$$\begin{aligned}
||u + s^\star||_{\omega,c} &\leq ||u||_{\omega,c} + ||s^\star||_{\omega,c} \\
&\leq ||u||_{\omega,c} + C_s \left|\left|\frac{2\omega^2}{c^2}u\right|\right| \\
&\leq \left(1 + \frac{2C_s\omega}{c_{min}}\right) ||u||_{\omega,c} \\
&\leq \left(1 + \frac{2C_s}{c_{min}}\right) \omega ||u||_{\omega,c}.
\end{aligned}$$

□

As explained in [1], it is interesting to use an approximation of the velocity parameter in numerical computations. In order to analyse the impact of this approximation, we consider stability of problem (2) under perturbations of the velocity parameter c. To this end, we introduce another velocity parameter c_ϵ satisfying Definition 1. In Theorem 3 we show that the distance between the operators $\mathcal{S}_{\omega,c}$ and $\mathcal{S}_{\omega,c_\epsilon}$ can be controlled by the distance between c and c_ϵ in an appropriate norm.

Before establishing Theorem 3, we need trace-like inequality (16), that we derive in Proposition 3.

Proposition 3. *For all $v \in H^1(0,Z)$, we have*

$$||v||_\infty \leq C_{tr}\omega^{-1/2}||v||_{\omega,c}, \tag{16}$$

with

$$C_{tr} = \max\left\{1, c_{max}\sqrt{\frac{1}{Z}+1}\right\}.$$

Proof. Let us first show that for all $v \in H^1(0,Z)$, the following estimate holds

$$||v||_\infty^2 \leq \frac{1}{Z}||v||^2 + 2||v||||v'||. \tag{17}$$

Indeed, for all $x, y \in (0,Z)$ there holds

$$|v(x)|^2 - |v(y)|^2 = \int_y^x \frac{d}{dz}\left(|v|^2\right)(\xi)d\xi = 2\mathrm{Re}\int_y^x v(\xi)\overline{v'(\xi)}d\xi \leq 2||v||||v'||.$$

We easily see that

$$|v(x)|^2 \leq |v(y)|^2 + 2||v||||v'||.$$

for all $x, y \in (0,Z)$. Integrating with respect to y, and dividing by Z, we have

$$|v(x)|^2 \leq \frac{1}{Z}||v||^2 + 2||v||||v'||,$$

and we obtain (17) by taking the supremum.

The proof now follows from (17) together with an $\epsilon-$inequality. Indeed, recalling that $\omega \geq 1$, we have:

$$\begin{aligned}
||v||_\infty^2 &\leq \frac{1}{Z}||v||^2 + \omega||v||^2 + \frac{1}{\omega}||v'||^2 \\
&\leq \omega^{-1}\left[\left(\frac{1}{Z}+1\right)\omega^2||v||^2 + ||v'||^2\right] \\
&\leq \omega^{-1}\max\left\{1, \left(\frac{1}{Z}+1\right)c_{max}^2\right\}||v||_{\omega,c}^2.
\end{aligned}$$

□

Theorem 3. *For all $f \in L^2(0,Z)$, there holds*

$$||\mathcal{S}_{\omega,c}f - \mathcal{S}_{\omega,c_\epsilon}f||_{\omega,c} \leq C_{s,c}\omega^2||c^{-2} - c_\epsilon^{-2}||_1||f||, \tag{18}$$

with

$$C_{s,c} = \frac{C_s C_{tr}^2}{C_\gamma}.$$

Proof. To simplify the notations, let us write $u = \mathcal{S}_{\omega,c} f$ and $u_\epsilon = \mathcal{S}_{\omega,c_\epsilon} f$. Since $B_{\omega,c}(u,v) = B_\epsilon(u_\epsilon, v)$ for all $v \in H^1(0,Z)$, there holds

$$B_{\omega,c}(u-u_\epsilon, v) = B_{\omega,c}(u_\epsilon, v) - B_\epsilon(u_\epsilon, v) = -\omega^2 \int_0^Z \left(\frac{1}{c(z)^2} - \frac{1}{c_\epsilon(z)^2} \right) u_\epsilon(z) \overline{v(z)} dz. \tag{19}$$

Let us bound the right hand side of (19). Using trace inequality (16) together with (6), we have

$$\begin{aligned} \left| \omega^2 \int_0^Z \left(\frac{1}{c(z)^2} - \frac{1}{c_\epsilon(z)^2} \right) u_\epsilon(z) \overline{v(z)} dz \right| &\leq \omega^2 ||c^{-2} - c_\epsilon^{-2}||_1 ||u_\epsilon||_\infty ||v||_\infty \\ &\leq C_{tr}^2 \omega ||c^{-2} - c_\epsilon^{-2}||_1 ||u_\epsilon||_{\omega,c_\epsilon} ||v||_{\omega,c} \\ &\leq C_s C_{tr}^2 \omega ||c^{-2} - c_\epsilon^{-2}||_1 ||f|| ||v||_{\omega,c}. \end{aligned}$$

We can conclude using (15). Indeed,

$$||u - u_\epsilon||_{\omega,c} \leq \frac{\omega}{C_\gamma} \sup_{v \in H^1(0,Z)} \frac{\text{Re } B_{\omega,c}(u-u_\epsilon, v)}{||v||_{\omega,c}} \leq \frac{C_{s,\epsilon}}{C_\gamma} \omega^2 ||c^{-2} - c_\epsilon^{-2}||_1 ||f||.$$

□

3. Finite element discretization

In this section, we recall the theory developed by Melenk and Sauter [8, 9] to derive asymptotic stability estimates. The main idea is that if the discrete space is sufficiently rich, the scheme is quasi-optimal.

Though the Helmholtz equation considered here is heterogeneous, the adaptation of the proofs of Melenk and Sauter is straightforward. For this reason, the proofs for the heterogeneous case are omitted in this paper.

The results of this section are abstract and general. In particular, they should carry over two-dimensional and three-dimensional problems without major modifications.

For the sake of simplicity, we will consider a uniform decomposition of the domain $(0,Z)$ together with polynomial basis functions with constant degree. To this end, we introduce a discretization step $h = 1/n_h$ with $n_h \in \mathbb{N}$, and the associated decomposition $t_j = jh$, for $j \in \{0, \dots, n_h\}$. Then we define the discretization space as

$$V^{h,p} = \left\{ v \in H^1(0,Z) \quad | \quad v|_{(t_{j-1},t_j)} \in \mathcal{P}_p,\ 0 \leq j \leq n_h \right\}, \tag{20}$$

where $1 \leq p \leq 3$ is a given integer and $\mathcal{P}_p$ stands for the space of polynomials of degree less than or equal to p.

We do not assume that the mesh fits the jumps of the wavespeed c. Thus, it is possible that c jumps inside a mesh cell. Though assuming that the mesh fits the jumps of c would greatly simplify the analysis, it is crucial to consider the general case. Indeed, if the medium is highly heterogeneous, fitting the jumps of c by refining the mesh might lead to

a heavy computational burden. In contrast, our analysis naturally covers coarse meshes, where the velocity parameter can arbitrarily change inside the cells.

In the following, we will need to quantify the ability of the discretization space $V^{h,p}$ to approximate solutions of the Helmholtz equation. In this regard, we introduce

$$\eta_{\omega,c}^{h,p} = \sup_{f\in L^2(0,Z)} \inf_{v_h\in V^{h,p}} \frac{||\mathcal{S}_{\omega,c}^{\star} f - v_h||_{\omega,c}}{||f||} = \sup_{f\in L^2(0,Z)} \inf_{v_h\in V^{h,p}} \frac{||\mathcal{S}_{\omega,c} f - v_h||_{\omega,c}}{||f||}. \tag{21}$$

In Theorem 4, we recall an important result of Melenk and Sauter: if $\omega\eta_{\omega,c}^{h,p}$ is controlled properly, the accuracy of the numerical scheme is ensured by approximation properties of the discretization space $V^{h,p}$.

Theorem 4. *Assume that $\omega\eta_{\omega,c}^{h,p} \leq \rho$. Then for all $f \in L^2(0,Z)$, there exists a unique element $\mathcal{S}_{\omega,c}^{h,p} f \in V^{h,p}$ such that*

$$B_{\omega,c}(\mathcal{S}_{\omega,c}^{h,p} f, v_h) = \int_0^Z f(z)\overline{v_h(z)}dz, \tag{22}$$

for all $v_h \in V^{h,p}$. Furthermore, there holds

$$||\mathcal{S}_{\omega,c} f - \mathcal{S}_{\omega,c}^{h,p} f||_{\omega,c} \leq C_e \eta_{\omega,c}^{h,p} ||f||. \tag{23}$$

The constants ρ and C_e are given by

$$\rho = \frac{c_{min}}{2(1+C_{tr})^2}, \quad C_e = \frac{2(1+C_{tr})^2 c_{max}}{c_{min}}.$$

4. Approximation properties

In the previous section, we have stated that the quality of the best approximation is crucial to obtain the quasi-optimality of the scheme. More precisely, the condition $\omega\eta_{\omega,c}^{h,p} \leq \rho$ is required.

Therefore, the aim of this section is to bound $\eta_{\omega,c}^{h,p}$ explicitly with respect to ω, h and p. This is done by building a good approximation of $\mathcal{S}_{\omega,c} f$ for a given $f \in L^2(0,Z)$. In the context of homogeneous media with a non-regular right hand side f in L^2, Melenk and Sauter have proposed a frequency-splitting of the solution to build the approximation [8, 9].

Here, we provide a methodology to construct an approximation of $\mathcal{S}_{\omega,c} f$ in the context of highly heterogeneous media. We are not aware of previous work dealing with discretization of Helmholtz problems with non-matching interfaces. To the best of our knowledge, our results are new.

The construction of our approximation is based on a splitting of $\mathcal{S}_{\omega,c} f$ into regular and non-regular parts. Lemmas 2 and 3 are devoted to the definition of the non-regular parts and the construction of their approximations. Then, in Theorem 5, we carry out the splitting of $\mathcal{S}_{\omega,c} f$ and obtain its actual approximation. That way, we are able to estimate $\eta_{\omega,c}^{h,p}$ for $1 \leq p \leq 3$. In Corollary 2, we use this estimate to obtain frequency explicit stability conditions and asymptotic error estimates for the numerical scheme induced by $V^{h,p}$.

The main novelties of this section are based on the use of special interpolation polynomials v_l^p that correspond to the jumps of the velocity parameter. These polynomials, introduced in Proposition 5, are the main reason why our analysis is currently limited to one-dimensional problems.

However, the author believes that with minor modifications, the proofs could carry over two-dimensional and three-dimensional problems in layered media. Indeed, considering a flat interface, special interpolation polynomials could be defined as a tensorial product of one-dimensional v_l^p interpolation polynomials in the direction normal to the interface, and standard interpolation polynomials in the tangential hyperplane.

It is also interesting to note that, strictly speaking, the hypothesis that the velocity is monotone is not required in this section. Indeed, we only need Corollary 1 and Proposition 1. We were not able to derive these two results without assuming that the velocity parameter is monotone. However, our results should apply unchanged for any propagation medium in which Corollary 1 and Proposition 1 hold.

For the sake of simplicity, we assume in the remaining of the paper that $\omega h \leq 1$. Note that this is a reasonable assumption which means that the number of discretization points per wavelength is bounded below.

Throughout this section, we will use standard approximation properties of polynomial functions. The required properties are summed up in Proposition 4.

Proposition 4. *Assume $1 \leq p \leq 3$. Then, for all $v \in H^{p+1}(0, Z)$, there exists an element $v_h \in V^{h,p}$ such that*

$$||v - v_h||_{\omega,c} \leq C_a h^p ||v^{(p+1)}||, \tag{24}$$

with

$$C_a = \sqrt{2} \max(1, \frac{1}{c_{min}}) \hat{C},$$

$\hat{C}$ being a numeric constant independent of all parameters.

Proof. Since $v \in H^{p+1}(0, Z)$, classical approximation theory ensures that there exists $v_h \in V^{h,p}$ such that

$$||v - v_h|| \leq \hat{C} h^{p+1} ||v^{(p+1)}||, \quad ||(v - v_h)'|| \leq \hat{C} h^p ||v^{(p+1)}||,$$

therefore

$$\begin{aligned} ||v - v_h||_{\omega,c}^2 &\leq \hat{C}^2 \left(\frac{\omega^2 h^{2p+2}}{c_{min}^2} + h^{2p} \right) ||v^{(p+1)}||^2 \\ &\leq \hat{C}^2 \max(1, \frac{1}{c_{min}^2})(1 + \omega^2 h^2) h^{2p} ||v^{(p+1)}||^2 \\ &\leq 2\hat{C}^2 \max(1, \frac{1}{c_{min}})^2 h^{2p} ||v^{(p+1)}||^2. \end{aligned}$$

□

Since we do not assume more than $L^2(0,Z)$ regularity for the right hand side, we might not expect the solution to be more than $H^2(0,Z)$. In Lemma 2 we isolate this non-regularity and define its approximation.

Lemma 2. *Let $f \in L^2(0,Z)$, there exists a function $\phi \in H_0^1(0,Z) \cap H^2(0,Z)$ such that $\phi'' = f$. Furthermore, there exists an element $\phi_h \in V_h^1$ such that*

$$||\phi - \phi_h||_{\omega,c} \leq C_a h ||f||.$$

Proof. Since the Laplace operator (second derivative in one dimension), is coercive, it is clear that there exists a unique function $\phi \in H_0^1(0,Z)$, such that $-\phi'' = -f$. Furthermore, the definition of ϕ ensures that $\phi \in H^2(0,Z)$ and $||\phi''|| = ||f||$. We conclude the proof with Proposition 4. □

The other source of irregularity in the solution are the discontinuities of the velocity parameter c. Lemma 3 presents one way to isolate those irregularities together with an approximation. But before introducing Lemma 3, we first define dedicated interpolation polynomials in Proposition 5.

Proposition 5. *For $p = 2$ or 3, consider the function $W_l^p \in L^2(0,Z)$ defined by*

$$W_l^p(z) = \frac{1}{p!}(z - z_l)^p 1_{z>z_l}.$$

We have $(W_l^p)^{(p+1)} = \delta_{z_l}$, and there exists a function $v_{l,h}^p \in V^{h,p}$ such that

$$||W_l^p - v_{l,h}^p||_{\omega,c} \leq C_{a,w} h^{p-1/2}, \tag{25}$$

with

$$C_{a,w} = 2\max(1, \frac{1}{c_{min}}).$$

Proof. First, it is clear that is $z_l = t_j$ for some integer j, then $W_l^p \in V^{h,p}$ and the proposition is trivial. Therefore, assume that $z_l \neq t_j$. There exist a unique integer $j_\star$ such that $t_{j\star} < z_l < t_{j_\star+1}$. We define

$$v_{l,h}^p|_{(t_{j-1},t_j)}(z) = \begin{cases} 0, & j < j_\star \\ \dfrac{1}{p!}(t_{j_\star} - z_l)^p \dfrac{(z - t_{j_\star-1})^p}{(t_{j_\star} - t_{j_\star-1})^p}, & j = j_\star \\ \dfrac{1}{p!}(z - z_l)^p, & j > j_\star. \end{cases}$$

One can easily verify that $v_{l,h}^p \in V^{h,p}$. Furthermore, we can show that $v_{l,h}^p$ satisfies (25) by direct computations. □

Lemma 3. *For $f \in L^2(0,Z)$, let us define*

$$\mu_2 = \omega^2 \sum_{l=1}^{L-1} \left[\frac{1}{c^2}\right]_l (\mathcal{S}_{\omega,c} f)(z_l) W_l^2, \quad \mu_3 = \omega^2 \sum_{l=1}^{L-1} \left[\frac{1}{c^2}\right]_l (\mathcal{S}_{\omega,c} f)'(z_l) W_l^3,$$

then we have

$$\mu_2^{(3)} = \omega^2 \sum_{l=1}^{L-1} \left[\frac{1}{c^2}\right]_l (\mathcal{S}_{\omega,c} f)(z_l)\delta_{z_l}, \quad \mu_3^{(4)} = \omega^2 \sum_{l=1}^{L-1} \left[\frac{1}{c^2}\right]_l (\mathcal{S}_{\omega,c} f)'(z_l)\delta_{z_l}.$$

Furthermore, there exist $\mu_{2,h} \in V_h^2$ *and* $\mu_{3,h} \in V_h^3$ *such that*

$$||\mu_2 - \mu_{2,h}||_{\omega,c} \leq C_{a,2}\omega h^{3/2}, \quad ||\mu_3 - \mu_{3,h}||_{\omega,c} \leq C_{a,3}\omega^2 h^{5/2},$$

with

$$C_{a,2} = C_{a,w}C_{s,j}, \quad C_{a,3} = C_{a,w}C_\infty \left(\frac{1}{c_{min}^2} - \frac{1}{c_{max}^2}\right).$$

Proof. The first part of the lemma is a direct consequence of the definition of the Dirac distribution δ. Therefore, let us focus on the construction of $\mu_{2,h}$ and $\mu_{3,h}$. We define

$$\mu_{2,h} = \omega^2 \sum_{l=1}^{L-1} \left[\frac{1}{c^2}\right]_l (\mathcal{S}_{\omega,c} f)(z_l) v_{l,h}^2.$$

In view of (25), it is clear that

$$||\mu_2 - \mu_{2,h}||_{\omega,c} \leq C_{a,w} \left(\sum_{l=1}^{L-1} \left[\frac{1}{c^2}\right]_l |(\mathcal{S}_{\omega,c} f)(z_l)|\right) \omega^2 h^{3/2}.$$

Therefore, using (7), we obtain

$$||\mu_2 - \mu_{2,h}||_{\omega,c} \leq C_{a,w}C_{s,j}\omega h^{3/2}||f||.$$

We define

$$\mu_{3,h} = \omega^2 \sum_{l=1}^{L-1} \left[\frac{1}{c^2}\right]_l (\mathcal{S}_{\omega,c} f)'(z_l) v_{l,h}^3,$$

and, using (25), we have

$$\begin{aligned} ||\mu_3 - \mu_{3,h}||_{\omega,c} &\leq C_{a,w} \left(\sum_{l=1}^{L-1} \left[\frac{1}{c^2}\right]_l (\mathcal{S}_{\omega,c} f)'(z_l)\right) \omega^2 h^{5/2} \\ &\leq C_{a,w} \left(\sum_{l=1}^{L-1} \left[\frac{1}{c^2}\right]_l\right) ||(\mathcal{S}_{\omega,c} f)'||_\infty \omega^2 h^{5/2}. \end{aligned}$$

Therefore, according to (12), we have

$$||\mu_3 - \mu_{3,h}||_{\omega,c} \leq C_{a,w}C_\infty \left(\frac{1}{c_{min}^2} - \frac{1}{c_{max}^2}\right) \omega^2 h^{5/2}||f||.$$

□

In Theorem 5 we combine approximations defined in Lemmas 2 and 3 to build the actual approximation of $\mathcal{S}_{\omega,c} f$. That way, we are able to bound $\eta_{\omega,c}^{h,p}$ for $1 \leq p \leq 3$.

Theorem 5. *Let $1 \leq p \leq 3$. There holds*

$$\eta_{h,p} \leq C_{\eta,p}\omega h, \tag{26}$$

with

$$C_{\eta,1} = C_a C_{s,2}, \quad C_{\eta,2} = C_a \max\left\{1, C_{a,2}, \frac{C_a C_s}{c_{min}^2}\right\}, \quad C_{\eta,3} = C_a \max\left\{1, C_{a,2}, C_{a,3}, \frac{C_a C_{s,2}}{c_{min}^2}\right\}.$$

Furthermore, assume that

$$\omega^{p+1} h^p \leq \rho_p, \tag{27}$$

where ρ_p is a constant depending on ρ and $C_{\eta,p}$ only, then the condition $\omega\eta_{h,p} \leq \rho$ is satisfied.

Proof. The case of linear approximation is easy. Indeed, recalling estimate (8), it is clear that there exists an element $v_{h,1} \in V_h^1$ such that

$$||\mathcal{S}_{\omega,c} f - v_{h,1}||_{\omega,c} \leq C_a h ||(\mathcal{S}_{\omega,c} f)''|| \leq C_a C_{s,2} \omega h ||f||,$$

therefore $\eta_{h,1} \leq C_a C_{s,a} \omega h$ and (26) and (27) immediately follows for $p = 1$.

We now turn to the case of higher polynomial degrees. Since $\mathcal{S}_{\omega,c} f$ is a weak solution to (1), we have

$$(\mathcal{S}_{\omega,c} f)'' = -f - \frac{\omega^2}{c^2} \mathcal{S}_{\omega,c} f,$$

so that, defining $\phi \in H^2(0, Z)$ as in Lemma 2,

$$(\mathcal{S}_{\omega,c} f - \phi)'' = -\frac{\omega^2}{c^2} \mathcal{S}_{\omega,c} f. \tag{28}$$

Differentiating (28) in the sense of distributions, we obtain

$$(\mathcal{S}_{\omega,c} f - \phi)^{(3)} = -\frac{\omega^2}{c^2} (\mathcal{S}_{\omega,c} f)' - \omega^2 \sum_{l=1}^{L-1} \left[\frac{1}{c^2}\right]_l (\mathcal{S}_{\omega,c} f)(z_l) \delta_{z_l},$$

so that, defining μ_2 as in Lemma 3

$$(\mathcal{S}_{\omega,c} f - \phi - \mu_2)^{(3)} = -\frac{\omega^2}{c^2} (\mathcal{S}_{\omega,c} f)'. \tag{29}$$

To conclude on the case of quadratic polynomials, we define $\theta_2 = \mathcal{S}_{\omega,c} f - \phi - \mu_2 \in H^3(0, Z)$. According to (29) and (6), we have

$$||\theta_2^{(3)}|| \leq \frac{\omega^2}{c_{min}^2} ||(\mathcal{S}_{\omega,c} f)'|| \leq \frac{C_s}{c_{min}^2} \omega^2 ||f||.$$

Therefore, there exists a function $\theta_{2,h} \in V_h^2$ such that

$$||\theta_2 - \theta_{2,h}||_{\omega,c} \leq \frac{C_a C_s}{c_{min}^2} \omega^2 h^2 ||f||.$$

We define $\phi_h \in V_h^1$ and $\mu_{2,h} \in V_h^2$ as in Lemma 2 and 3 and $v_{h,2} = \phi_h + \mu_{2,h} + \theta_{2,h}$. Since $\mathcal{S}_{\omega,c} f = \phi + \mu_2 + \theta_2$, we obtain

$$||\mathcal{S}_{\omega,c} f - v_{h,2}||_{\omega,c} \leq \left(C_a h + C_{a,2} \omega h^{3/2} + \frac{C_a C_s}{c_{min}^2} \omega^2 h^2 \right) ||f||,$$

and (26) follows for $p = 2$ because $\omega \geq 1$ and $\omega h \leq 1$. We now derive (27) for $p = 2$. There holds

$$\begin{aligned} \omega \eta_{h,2} &\leq C_{\eta,2} \left(\omega h + \omega^2 h^{3/2} + \omega^3 h^2 \right) \\ &\leq C_{\eta,2} \left(\omega^{-1/2} (\omega^3 h^2)^{1/2} + (\omega h)^{1/2} (\omega^3 h^2)^{1/2} + \omega^3 h^2 \right). \end{aligned}$$

Thus, since $\omega^{-1/2} \leq 1$ and $(\omega h)^{1/2} \leq 1$, assuming that $\omega^3 h^2 \leq \rho_2$, we have

$$\omega \eta_{h,2} \leq C_{\eta,2} \left(2\rho_2^{1/2} + \rho_2 \right),$$

and selecting

$$\rho_2 = \left(\left(\frac{\rho}{C_{\eta,2}} + 1 \right)^{1/2} - 1 \right)^2,$$

we have $\omega \eta_{h,2} \leq \rho$.

We now turn to the case $p = 3$. We differentiate (29) again and obtain

$$(\mathcal{S}_{\omega,c} f - \phi - \mu_2)^{(4)} = -\frac{\omega^2}{c^2} (\mathcal{S}_{\omega,c} f)'' - \omega^2 \sum_{l=1}^{L-1} \left[\frac{1}{c^2} \right]_l (\mathcal{S}_{\omega,c} f)'(z_l) \delta_{z_l},$$

so that, defining μ_3 as in Lemma 3, we have

$$(\mathcal{S}_{\omega,c} f - \phi - \mu_2 - \mu_3)^{(4)} = -\frac{\omega^2}{c^2} (\mathcal{S}_{\omega,c} f)''. \tag{30}$$

To conclude, we define $\theta_3 = \mathcal{S}_{\omega,c} f - \phi - \mu_2 - \mu_3 \in H^4(0, Z)$, so that $\mathcal{S}_{\omega,c} f = \phi + \mu_2 + \mu_3 + \theta_3$ and

$$||\theta_3^{(4)}|| \leq \frac{\omega^2}{c_{min}^2} ||(\mathcal{S}_{\omega,c} f)''|| \leq \frac{C_{s,2}}{c_{min}^2} \omega^3 ||f||.$$

Let $\theta_{3,h} \in V_h^3$ be the best approximation to θ_3 and define $\mu_{3,h} \in V_h^3$ as in Lemma 3. We define $v_{h,3} = \phi_h + \mu_{2,h} + \mu_{3,h} + \theta_{3,h} \in V_h^3$, and then we have

$$||\mathcal{S}_{\omega,c} f - v_{h,3}||_{\omega,c} \leq \left(C_a h + C_{a,2} \omega h^{3/2} + C_{a,3,h} \omega^2 h^{5/2} + \frac{C_a C_{s,2}}{c_{min}^2} \omega^3 h^3 \right) ||f||,$$

and we obtain (26) and (27) for $p = 3$ with same arguments than in the quadratic case. □

With the bound on $\eta_{\omega,c}^{h,p}$, we are now able to deliver frequency explicit stability conditions and error estimates.

Corollary 2. *Let $1 \leq p \leq 3$. Assume that $\omega^{p+1} h^p \leq \rho_p$. Then there is a unique numerical solution $\mathcal{S}_{\omega,c}^{h,p} f$ and the following error estimate holds*

$$||\mathcal{S}_{\omega,c} f - \mathcal{S}_{\omega,c}^{h,p} f||_{\omega,c} \leq C_{e,p} \omega h ||f||,$$

where

$$C_{e,p} = C_e C_{\eta,p}.$$

Proof. The proof is a direct application of Theorem 4 and Theorem 5. Indeed, assuming $\omega^{p+1}h^p \leq \rho_p$, (27) yields $\omega\eta_{\omega,c}^{h,p} \leq \rho$ and we can use Theorem 4. The result directly follows from (23) because we also have $\eta_{w,c}^{h,p} \leq C_{\eta,p}\omega h$ from (26). □

Theorem 5 and Corollary 2 are derived without assuming that the mesh fits the jumps of the wavespeed c. On the one hand, it is probably possible to extend the above results to arbitrary p by assuming that the wavespeed is constant inside each cell. In this case, we would derive results similar to those obtained by Melenk and Sauter [8, 9]. On the other hand, it is usually not possible to fit the wavespeed with the mesh in applications.

Since the aim of the present paper is to focus on highly heterogeneous media, our choice is to provide results that are restricted to the case $p \leq 3$, but valid even for large mesh steps $h > \nu$ (we recall that ν stands for the length of the smallest layer of the wavespeed). The other possibility would be to consider arbitrary p, but small mesh steps $h < \nu$.

5. Multiscale medium approximation

In Sections 3 and 4, we derived frequency explicit stability conditions and asymptotic error estimates assuming that we are able to solve problem (22) exactly. It implies that we are able to compute the coefficients of the linear system, including the integrals

$$\int_0^Z \frac{1}{c^2(z)}\phi_h(z)\overline{\psi_h(z)}dz, \tag{31}$$

for all basis functions $\phi_h, \psi_h \in V^{h,p}$ of $V^{h,p}$. Of course, in a one-dimensional space, it is always possible to evaluate this integral analytically, since it can be decomposed into several intervals where c is constant. However, as pointed out in [1], this is not the case in two-dimensional domains. Furthermore, even when the analytical formula is available (for example, if we assume that the interfaces defining c are polygons in 2D), it might be expensive to compute, since the quadrature scheme used will be different in each cell.

We propose a different approach which consists in approximating c by another parameter c_ϵ designed so that the integrals (31) are always cheap to compute numerically. We construct c_ϵ so that Definition 1 is satisfied. Hence, Theorem 3 will ensure the quality of the numerical approximation. We call this process the Multiscale Medium Approximation method (MMAm), because the scale ϵ of the medium approximation is independent of the scale h of the finite element approximation.

We now tackle the construction of c_ϵ. We suppose that the velocity parameter c satisfies Definition 1 and that

$$\min_{l\in\{1,\dots,L\}} z_l - z_{l-1} > 2\nu. \tag{32}$$

We use discretization space (20) with $n \in \mathbb{N}^\star$ cells. We consider $m \in \mathbb{N}^\star$ subdivisions of each cell of our mesh. Then, for $i \in \{1, \dots, n\}$ and $j \in \{1, \dots, m\}$

$$c_\epsilon|_{(t_i^{j-1}, t_i^j)} = \sup_{(t_i^{j-1}, t_i^j)} c$$

where $t_i^j = t_i + j\epsilon h$, and $\epsilon = 1/m$. Note that, because of (32), it is clear that both c and c_ϵ satisfy Definition 1 as soon as $h\epsilon < \nu$. In Lemma 4 we show that the medium is properly approximated if $h\epsilon$ is small enough.

Lemma 4. *Assume that $h\epsilon < \nu$, then there holds*

$$|c^{-2} - c_\epsilon^{-2}|_1 \leq (c_{min}^{-2} - c_{max}^{-2}) h\epsilon. \tag{33}$$

Proof. For each $l \in \{1, \dots, L-1\}$, there exists a unique pair $i_l \in \{1, \dots, n\}$ and $j_l \in \{1, \dots, m\}$ such that $z_l \in [t_{i_l}^{j_l - 1}, t_{i_l}^{j_l})$. Furthermore, since $h\epsilon < \nu$, $i_l \neq i_k$ and $j_l \neq j_k$ if $j \neq k$. If $i \neq i_l$ and $j \neq j_l$ for all $l \in \{1, \dots, L-1\}$, c is constant on (t_i^{j-1}, t_i^j) and therefore $c_\epsilon = c$ on this interval. It follows that

$$|c^{-2} - c_\epsilon^{-2}|_1 = \sum_{l=1}^{L-1} \int_{t_{i_l}^{j_l - 1}}^{t_{i_l}^{j_l}} |c^{-2}(z) - c_\epsilon^{-2}(z)| dz \leq h\epsilon \sum_{l=1}^{L-1} \left[\frac{1}{c^2}\right]_l \leq h\epsilon \left(c_{min}^{-2} - c_{max}^{-2}\right).$$

□

In Theorem 6, we conclude about the convergence of the MMAm.

Theorem 6. *Assume that $h\epsilon < \nu$ and $\omega^{p+1} h^p \leq \rho_p$. Then for all $f \in L^2(0, Z)$, there exists a unique element $\mathcal{S}_{\omega, c_\epsilon}^{h,p} f \in V^{h,p}$ such that*

$$B_{\omega, c_\epsilon}(\mathcal{S}_{\omega, c_\epsilon}^{h,p} f, v) = \int_0^Z f(z)\overline{v(z)} dz, \tag{34}$$

for all $v \in V^{h,p}$. Furthermore, there holds

$$||\mathcal{S}_{\omega,c} f - \mathcal{S}_{\omega, c_\epsilon}^{h,p} f||_{\omega,c} \leq C_{e,p,\epsilon}(\omega h + \omega^2 h\epsilon)||f||, \tag{35}$$

with

$$C_{e,p,\epsilon} = \max\left\{(c_{min}^{-2} - c_{max}^{-2}) C_{s,c}, \frac{c_{max} C_{e,p}}{c_{min}}\right\}.$$

Proof. Using Lemma 4, the result directly follows from (18), (33), the bounds (26) and (27) from Corollary 2 and the error estimate (23) of Theorem 4:

$$\begin{aligned}
||\mathcal{S}_{\omega,c} f - \mathcal{S}_{\omega, c_\epsilon}^{h,p} f||_{\omega,c} &\leq ||\mathcal{S}_{\omega,c} f - \mathcal{S}_{\omega, c_\epsilon} f||_{\omega,c} + ||\mathcal{S}_{\omega, c_\epsilon} f - \mathcal{S}_{\omega, c_\epsilon}^{h,p} f||_{\omega,c} \\
&\leq ||\mathcal{S}_{\omega,c} f - \mathcal{S}_{\omega, c_\epsilon} f||_{\omega,c} + \frac{c_{max}}{c_{min}} ||\mathcal{S}_{\omega, c_\epsilon} f - \mathcal{S}_{\omega, c_\epsilon}^{h,p} f||_{\omega, c_\epsilon} \\
&\leq C_{s,c}\omega^2 ||c^{-2} - c_\epsilon^{-2}||_1 ||f|| + \frac{c_{max} C_{e,p}}{c_{min}} \omega h ||f|| \\
&\leq \left(C_{s,c}(c_{min}^{-2} - c_{max}^{-2})\omega^2 h\epsilon + \frac{c_{max} C_{e,p}}{c_{min}} \omega h\right) ||f||.
\end{aligned}$$

□

We close this section by discussing the computational cost of the MMAm, as compared to the standard FEm. As already observed, the main difference between the standard FEm and the MMAm is the way the integrals

$$\int_0^Z \frac{1}{c^2(z)}\phi_h(z)\overline{\psi_h(z)}dz, \tag{36}$$

are computed, for each combination of basis functions $\phi_h, \psi_h \in V_h^p$.

In order to give an insight of the overhead induced by the MMAm as compared to the standard FEm, we briefly explain how (36) is computed in the FEm and in the MMAm. Though we focus on the 1D case here, our analysis is valid for 2D and 3D as long as the mesh cells are obtained from the reference one through affine mappings. For instance, the computational cost for 2D problems with triangular meshes is analysed in [1].

Let us first recall how the finite element space V_h^p is actually constructed. First, we introduce the Lagrangian basis $\{\hat{l}_\mu\}_{\mu=1}^{p+1}$ of the reference cell $(0,1)$. It is defined by $\hat{l}_\mu \in \mathcal{P}_p(0,1)$ and

$$\hat{l}_\mu(\frac{\lambda-1}{p}) = \delta_{\mu\lambda},$$

for $\mu, \lambda \in \{1, \dots, p+1\}$.

Then, considering a basis function $\phi_h \in V_h$ and a mesh cell (t_{j-1}, t_j), either $\phi_h|_{(t_{j-1},t_j)} = 0$ or

$$\phi_h|_{(t_{j-1},t_j)}(z) = \hat{l}_\mu(\frac{z-t_{j-1}}{t_j - t_{j-1}}),$$

for some $\mu \in \{1, \dots, p+1\}$. Thus, it is clear that computing (36) for every combination of basis functions amounts to computing the integrals

$$\int_{t_{j-1}}^{t_j} \frac{1}{c^2(z)}\hat{l}_\mu(\frac{z-t_{j-1}}{t_j-t_{j-1}})\hat{l}_\lambda(\frac{z-t_{j-1}}{t_j-t_{j-1}})dz, \tag{37}$$

for $1 \le j \le n$ and $1 \le \lambda, \mu \le p+1$.

In finite element analysis, a key idea to speed up the computation of (37) (and thus, the construction of the linear system), is to precompute quantities involving the Lagrangian basis of the reference cell. In the standard FEm, the reference values

$$\hat{M}_{\mu\lambda} = \int_0^1 \hat{l}_\mu(\hat{z})\hat{l}_\lambda(\hat{z})d\hat{z},$$

are computed for $1 \leq \lambda, \mu \leq p+1$. Then, because c is assumed to be constant inside each cell, introducing $\hat{z} = (z - t_{j-1})/(t_j - t_{j-1})$ we can compute (37) with

$$\begin{aligned}\int_{t_{j-1}}^{t_j} \frac{1}{c^2(z)} \hat{l}_\mu(\frac{z-t_{j-1}}{t_j - t_{j-1}}) \hat{l}_\lambda(\frac{z-t_{j-1}}{t_j - t_{j-1}}) dz &= \frac{1}{c_j^2} \int_{t_{j-1}}^{t_j} \hat{l}_\mu(\frac{z-t_{j-1}}{t_j - t_{j-1}}) \hat{l}_\lambda(\frac{z-t_{j-1}}{t_j - t_{j-1}}) dz \\ &= \frac{t_j - t_{j-1}}{c_j^2} \int_0^1 \hat{l}_\mu(\hat{z}) \hat{l}_\lambda(\hat{z}) d\hat{z} \\ &= \frac{h}{c_j^2} \hat{M}_{\mu\lambda},\end{aligned}$$

where c_j is the value of c over (t_{j-1}, t_j).

The technique used in the MMAm mimics the standard FEm technique, but allows c to take m different values inside each cell. Accordingly, the reference values

$$\hat{M}^i_{\mu\lambda} = \int_{\hat{t}^{i-1}}^{\hat{t}^i} \hat{l}_\mu(\hat{z}) \hat{l}_\lambda(\hat{z}) d\hat{z},$$

with $\hat{t}^i = i/m$ are computed for $1 \leq i \leq m$ and $1 \leq \lambda, \mu \leq p+1$.

We emphasize that computing the reference values $\hat{M}^i_{\mu\lambda}$ is a very cheap task. Indeed, the computations need to be done only for the reference cell. In particular, the computational cost is the same for all mesh steps h.

Once the reference values have been computed, we follow the same guidelines that the standard FEm to compute (37) efficiently:

$$\begin{aligned}\int_{t_{j-1}}^{t_j} \frac{1}{c^2(z)} \hat{l}_\mu(\frac{z-t_{j-1}}{t_j - t_{j-1}}) \hat{l}_\lambda(\frac{z-t_{j-1}}{t_j - t_{j-1}}) dz &= \sum_{i=1}^m \int_{t_j^{i-1}}^{t_j^i} \frac{1}{c^2(z)} \hat{l}_\mu(\frac{z-t_{j-1}}{t_j - t_{j-1}}) \hat{l}_\lambda(\frac{z-t_{j-1}}{t_j - t_{j-1}}) dz \\ &= \sum_{i=1}^m \frac{1}{c_{j,i}^2} \int_{t_j^{i-1}}^{t_j^i} \hat{l}_\mu(\frac{z-t_{j-1}}{t_j - t_{j-1}}) \hat{l}_\lambda(\frac{z-t_{j-1}}{t_j - t_{j-1}}) dz \\ &= (t_j - t_{j-1}) \sum_{i=1}^m \frac{1}{c_{j,i}^2} \int_{\hat{t}^{i-1}}^{\hat{t}^i} \hat{l}_\mu(\hat{z}) \hat{l}_\lambda(\hat{z}) d\hat{z} \\ &= h \sum_{i=1}^m \frac{1}{c_{j,i}^2} \hat{M}^i_{\mu\lambda},\end{aligned}$$

where $c_{i,j}$ is the value of c over (t_j^{i-1}, t_j^i).

Considering one cell, the standard FEm requires to weight the reference value by a multiplication with the unique value of the velocity over this cell. In comparison, in the MMAm, the weighting amounts to a scalar product between the m reference values and the m values of of the velocity on the cell.

In terms of complexity estimates, if we consider a problem set in $\mathbb{R}^d$ the computational cost for building the linear system in the standard FEm is $\mathcal{O}(np^{2d})$, where n is the number of mesh cells, p. If we use the MMAm with m quadrature subcells, the computational

complexity is $\mathcal{O}(mnp^{2d})$. These complexity estimates remain true for 2D and 3D computations. The only limitation is the use of affine maps, which include triangular and tetrahedral meshes.

As a result, assembling the MMAm linear system is m times more costly than assembling the standard FEm system. However, we point out that this is only a minor drawback. Indeed, this step can be trivially parallelized, since all computations are local and no communication is required between cells.

Furthermore, we state from [2] that the matrix factorization of a 3D finite-element problem has complexity $\mathcal{O}(n^2p^6)$. As a result, in 3D applications, the computational time required for assembling the matrix is orders of magnitude below that required for factorizing the matrix. Therefore, even if an important number of subcells m is used in the MMAm, the computational time for building the linear system is negligible as compared to the computational time required for factorizing the matrix. More precisely, we see that the overhead of the MMAm is negligible as soon as $m \ll n$.

We conclude that for large 3D problems, the overhead of the MMAm is insignificant.

6. 1D Numerical Experiments

In this section, we will consider the following problem,

$$\left\{\begin{array}{rcl} -\dfrac{\omega^2}{c^2(z)}u(z) - u''(z) &=& 0, \quad z \in (0,1), \\ -u'(0) - \dfrac{\mathbf{i}\omega}{c(0)}u(0) &=& 1, \\ u'(1) - \dfrac{\mathbf{i}\omega}{c(1)}u(1) &=& 0, \end{array}\right. \tag{38}$$

for different parameters c. The domain is scaled to the unit domain $(0,1)$ and we use values ranging from 1 to 5 for the velocity. This is consistent with geophysical applications where we can consider a depth of $1000m$ and velocity values ranging from $1000m.s^{-1}$ to $5000m.s^{-1}$.

We consider six different velocity models represented by $c^{(i)}$ for $i \in \{1,\dots,6\}$. The first two are monotone and satisfy Definition 1, the others are not and therefore violate the hypothesis of our theoretical analysis. We further point out that the length ν^i of the thinest layer of the model is decreasing from one experiment to the other. We have constructed all velocity models except from the first so that the length of each layer is different and can not be fitted by a regular mesh. It ensures that we do not accidentally obtain an exact approximation of the velocity parameter when using the MMAm. The layers of the velocity parameters are given by

$$z_0 = 0, \quad z_1 = 0.5, \quad z_2 = 1,$$

for Experiment 1,

$$z_0 = 0, \quad z_l = \frac{l + 0.4\cos l}{L} \quad (0 < l < L), \quad z_L = 1,$$

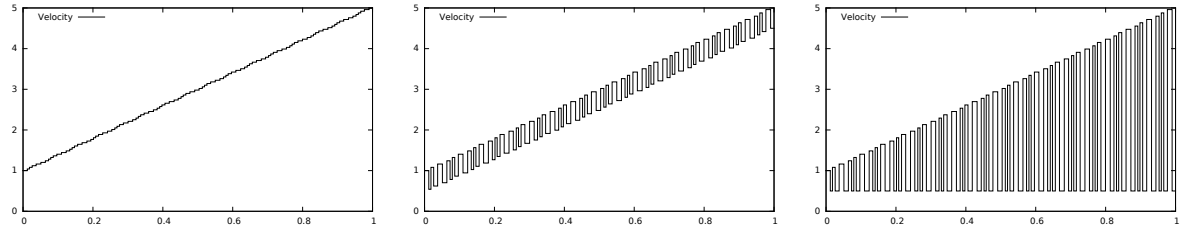

FIGURE 1. Velocity parameters used in Experiments 2, 3 and 4

with $L = 100$ for Experiments 2, 3 and 4 and with $L = 1000$ for Experiments 5 and 6.

In Experiment 1, we focus on a simple two-layered medium:

$$c^{(1)}(z) = \begin{cases} 1 & \text{if } z < 0.5 \\ 2 & \text{if } z > 0.5, \end{cases}$$

then, in Experiment 2, we consider an increasing velocity parameter (see also Figure 1)

$$c_l^{(2)} = 1 + 4\frac{l-1}{99}.$$

In Experiments 3 and 4, we perturb the parameter $c^{(2)}$ one layer over two to create a more complex medium (see Figure 1).

$$c_l^{(3)} = \begin{cases} 1 + 4\dfrac{l-1}{99}, & l \text{ odd} \\ 1 + 4\dfrac{l-1}{99} - 0.5, & l \text{ even} \end{cases} \qquad c_l^{(4)} = \begin{cases} 1 + 4\dfrac{l-1}{99}, & l \text{ odd} \\ 0.5, & l \text{ even.} \end{cases}$$

Finally, the velocity parameters of Experiments 5 and 6 are similar to Experiments 3 and 4, but with 1000 layers instead of 100.

$$c_l^{(5)} = \begin{cases} 1 + 4\dfrac{l-1}{999}, & l \text{ odd} \\ 1 + 4\dfrac{l-1}{999} - 0.5, & l \text{ even} \end{cases} \qquad c_l^{(6)} = \begin{cases} 1 + 4\dfrac{l-1}{999}, & l \text{ odd} \\ 0.5, & l \text{ even.} \end{cases}$$

We tabulate the relative L^2 error $||u-u_h||/||u||$ for different frequencies ω, mesh steps $h = 1/n$ and multiscale subdivisions m. First, we investigate frequency explicit requirements for meshing. The three first test-cases show that in the case where the medium is slowly variating, the pre-asymptotic error estimate in $\mathcal{O}(\omega^{2p+1}h^{2p})$ known in the homogeneous case is still valid and optimal, provided that the medium is properly approximated (see Tables 1 to 3). However Experiment 4 shows that this is no longer the case for more complex media (see Table 4).

The other aim of our study is to figure out which order of discretization is the cheapest for a given accuracy and frequency. In the three first experiments we see that for a given accuracy and frequency, the number of degrees of freedom required decreases when the order is increasing, showing the efficiency of high order methods. For the other experiments, the

situation is more complex and is described in Table 5. Nevertheless, we observe that for a given accuracy, the number of degrees of freedom required for $p = 4$ is always less than for $p = 1, 2, 3$.

We can make an additional comment which do not directly apply to the method in higher dimensions. We can use static condensation on the degrees of freedom inside one cell (they only depends on the values at the vertices, see [6]) and reduce the size of the global linear system to $n \times n$. In this situation, high order methods look even more attractive, since the number of cells required for a given accuracy is clearly decreasing when the order is increasing.

6.1. **Experiment 1: Two-layered gradient.** We consider (38) with the parameter $c^{(1)}$ and solve it with three different methodologies. First, we use a mesh with an even number of cells which fits the interface of the velocity parameter. Then we use a mesh with an odd number of cells, so that there is a velocity contrast in the middle cell of the mesh. With the non-fitting mesh, we first run simulations without multiscale medium approximation: $c_\epsilon^{(1)}$ is taken constant in each cell ($m = 1$), and the medium is approximated in the middle cell. Then, we use two subcells per cell ($m = 2$) to approximate the velocity, so that the medium is perfectly represented. We run our experiments with p ranging from 1 to 6 for different frequencies, using the rule $\omega^{2p+1}h^{2p} \leq C$. In Table 1, we present the relative error on the numerical solution, for the three different techniques: "even" refers to the fitting mesh, "odd1" to the non-fitting with $m = 1$ and "odd2" to the non-fitting mesh with $m = 2$.

We can make the following comments: it is clear that the meshing strategy $\omega^{2p+1}h^{2p} \leq C$ is optimal since the error remains constant when ω is increasing for all tables. In addition, the tables show that for a given frequency, high order methods require less degrees of freedom for a given accuracy. Then, we see that when the subquadrature technique is used, the results obtain with the non-fitting mesh are comparable to those obtain with the fitting one. Finally, apart from the case of $p = 1$, the results on the non-fitting mesh are always improved when using $m = 2$ subcells. It shows that for high order methods, the medium approximation error can be larger than the best approximation error.

6.2. **Experiment 2: 100 layered gradient.** We now consider the velocity parameter $c^{(2)}$, which features 100 layers.

We solve the problem with finite elements ranging from $p = 1$ to $p = 6$ together with the meshing condition $\omega^{2p+1}h^{2p} \leq C$. The results are presented with different number of subcells $m = 1, 10$ and 100.

To start with, we can make the same comment than the previous experiment. The meshing strategy $\omega^{2p+1}h^{2p} \leq C$ is enough to ensure the precision of the method. Furthermore, for a given frequency, higher order methods give an equivalent result with less degrees of freedom.

In most cases, increasing the number of subcells improve the precision of the numerical scheme as expected. However, for $p = 3, 4, 5$ especially at high frequency, this is not the case. This can be explained by the fact that in those cases, the mesh is fine enough to

$\mathcal{P}_1$					
ω	ndf	n	even	odd1	odd2
5	10	12	2.37e-02	1.29e-01	2.80e-02
10	30	32	2.20e-02	7.72e-02	2.33e-02
50	352	354	1.99e-02	2.51e-02	2.00e-02
100	1000	1001	1.97e-02	1.55e-02	1.98e-02
500	11180	11181	1.98e-02	1.15e-02	1.98e-02
$\mathcal{P}_2$					
ω	ndf	n	even	odd1	odd2
50	32	100	8.32e-02	3.51e-01	9.93e-02
100	78	238	7.89e-02	2.84e-01	8.61e-02
500	590	1774	7.90e-02	1.71e-01	8.06e-02
1000	1404	4216	7.97e-02	1.36e-01	8.05e-02
2000	3342	10030	8.01e-02	1.07e-01	8.05e-02

$\mathcal{P}_5$					
ω	ndf	n	even	odd1	odd2
200	42	379	1.67e-02	9.16e-01	2.61e-02
500	116	1045	1.66e-02	8.61e-01	2.15e-02
1000	248	2242	1.79e-02	8.26e-01	2.12e-02
5000	1464	13177	1.91e-02	7.45e-01	2.04e-02
10000	3138	28252	1.98e-02	7.11e-01	2.07e-02
$\mathcal{P}_6$					
ω	ndf	n	even	odd1	odd2
200	34	375	7.93e-03	1.06e+00	2.26e-02
500	92	1024	9.70e-03	9.97e-01	1.71e-02
1000	196	2168	1.11e-02	9.54e-01	1.45e-02
5000	1128	12420	1.49e-02	8.74e-01	1.16e-02
10000	2392	26324	1.69e-02	8.43e-01	1.11e-02

TABLE 1. Relative L^2 error in Experiment 1

$\mathcal{P}_1$					
ω	n	ndf	m=1	m=10	m=100
5	5	6	4.48e-02	1.91e-02	2.01e-02
10	15	16	2.94e-02	1.64e-02	1.83e-02
50	176	177	1.17e-02	1.69e-02	1.64e-02
100	500	501	1.43e-02	1.63e-02	1.63e-02
500	5590	5591	1.52e-02	1.60e-02	1.63e-02
$\mathcal{P}_2$					
ω	n	ndf	m=1	m=10	m=100
50	22	67	6.07e-02	5.01e-02	4.31e-02
100	52	157	5.16e-02	4.87e-02	4.66e-02
500	394	1183	5.73e-02	4.79e-02	4.75e-02
1000	937	2812	7.10e-02	4.97e-02	4.83e-02
2000	2229	6688	9.29e-02	4.97e-02	4.89e-02

$\mathcal{P}_5$					
ω	n	ndf	m=1	m=10	m=100
200	28	253	1.93e-01	9.02e-02	3.23e-02
500	77	694	8.29e-02	7.39e-02	3.50e-02
1000	166	1495	3.97e-01	5.64e-02	3.72e-02
5000	976	8785	3.49e-01	4.54e-02	4.67e-02
10000	2093	18838	4.10e-02	5.67e-02	5.05e-02
$\mathcal{P}_6$					
ω	n	ndf	m=1	m=10	m=100
200	22	243	1.13e-01	5.90e-02	2.94e-02
500	59	650	7.86e-02	3.66e-02	3.98e-02
1000	127	1398	1.78e-01	5.04e-02	3.86e-02
5000	726	7987	8.35e-02	7.05e-02	4.93e-02
10000	1538	16919	1.41e-01	7.26e-02	5.44e-02

TABLE 2. Relative L^2 error in Experiment 2

capture the variations of the velocity, and improving the approximation of the medium does not improve the accuracy of the numerical solution. The error is then increasing a little because of numerical error due to finite precision arithmetic.

6.3. **Experiment 3: 100 layered gradient with perturbations.** The velocity parameter used for the experiment is $c^{(3)}$. Numerical results are presented in Table 3.

We use the meshing condition $\omega^{2p+1}h^{2p} \leq C$ and observe that for $1 \leq p \leq 6$, the error on the numerical solution remains bounded. However, we see than the error is not "constant", but varies from one frequency to another, more than in the previous experiments. We observe again than for a given frequency, higher order discretizations require less degrees of freedom for a given accuracy.

$\mathcal{P}_1$					
ω	n	ndf	m=10	m=100	m=1000
50	353	354	2.26e-02	1.19e-02	1.30e-02
100	1000	1001	2.84e-02	1.16e-02	1.29e-02
200	2828	2829	1.50e-02	9.19e-03	9.48e-03
500	11180	11181	1.03e-02	1.22e-02	1.24e-02
1000	31622	31623	7.09e-03	1.02e-02	1.03e-02
2000	89442	89443	4.40e-03	5.20e-03	5.26e-03
$\mathcal{P}_2$					
ω	n	ndf	m=10	m=100	m=1000
50	44	133	8.52e-02	4.47e-02	3.69e-02
100	105	316	1.36e-01	3.13e-02	3.37e-02
200	250	751	5.32e-02	3.06e-02	3.60e-02
500	788	2365	7.77e-02	3.30e-02	4.27e-02
1000	1874	5623	7.77e-02	2.67e-02	2.55e-02
2000	4458	13375	4.16e-02	1.03e-02	1.25e-02
5000	14014	42043	2.70e-02	3.33e-02	2.83e-02

$\mathcal{P}_5$					
ω	n	ndf	m=10	m=100	m=1000
200	67	604	3.05e-01	4.92e-02	3.33e-02
500	186	1675	1.19e-01	2.64e-02	2.73e-02
1000	399	3592	1.86e-01	2.63e-02	2.10e-02
2000	855	7696	9.52e-02	1.44e-02	1.45e-02
5000	2343	21088	6.52e-02	5.45e-03	1.34e-02
10000	5023	45208	6.22e-02	5.47e-03	3.16e-03
$\mathcal{P}_6$					
ω	n	ndf	m=10	m=100	m=1000
200	51	562	1.95e-01	1.08e-02	2.21e-02
500	139	1530	4.29e-01	3.40e-02	4.93e-02
1000	296	3257	3.54e-01	2.40e-02	2.16e-02
2000	628	6909	7.96e-02	4.73e-02	2.05e-02
5000	1694	18635	2.11e-01	5.32e-02	1.73e-02
10000	3590	39491	4.41e-01	2.71e-02	1.49e-02

TABLE 3. Relative L^2 error in Experiment 3

$\mathcal{P}_1$					
ω	n	ndf	m=10	m=100	m=1000
50	707	708	1.31e-01	5.38e-02	5.65e-02
100	2000	2001	2.72e-03	1.85e-03	1.91e-03
200	5656	5657	1.92e-03	1.16e-03	1.53e-03
500	22360	22361	1.46e-02	8.59e-03	9.17e-03
1000	63245	63246	5.46e-02	3.51e-02	3.66e-02
2000	178885	178886	9.33e-02	8.28e-02	8.39e-02
$\mathcal{P}_2$					
ω	n	ndf	m=10	m=100	m=1000
50	132	397	2.04e-01	8.84e-02	9.69e-02
100	316	949	1.39e-02	3.29e-03	8.49e-04
200	752	2257	1.91e-02	1.64e-03	8.46e-04
500	2364	7093	5.28e-02	1.34e-02	5.09e-03
1000	5623	16870	2.26e+00	1.68e-02	1.64e-02
2000	13374	40123	9.29e-02	5.77e-02	3.02e-02
5000	42044	126133	3.00e-03	8.17e-04	2.71e-04

$\mathcal{P}_5$					
ω	n	ndf	m=10	m=100	m=1000
200	135	1216	1.51e-01	1.45e-02	7.97e-03
500	372	3349	2.54e-01	4.33e-02	2.03e-02
1000	798	7183	8.46e-01	7.32e-02	9.86e-02
2000	1710	15391	1.50e+00	2.66e-01	1.75e-01
5000	4687	42184	5.16e-02	3.93e-03	1.05e-03
10000	10047	90424	8.39e-01	7.09e-02	6.06e-02
$\mathcal{P}_6$					
ω	n	ndf	m=10	m=100	m=1000
200	103	1134	6.94e-02	1.41e-02	4.84e-03
500	279	3070	3.74e-01	5.01e-02	2.07e-02
1000	592	6513	8.66e-01	2.06e-01	5.67e-02
2000	1256	13817	3.05e+00	3.31e-01	1.39e-01
5000	3389	37280	6.98e-02	4.47e-03	1.57e-03
10000	7181	78992	1.23e+00	3.09e-01	5.97e-02

TABLE 4. Relative L^2 error in Experiment 4

6.4. **Experiment 4: 100 layered gradient with rough perturbations.** We now use the velocity parameter $c^{(5)}$. Numerical results are presented in Table 4.

We see that the error is varying a lot depending on the frequency when $\omega^{2p+1}h^{2p}$ is kept constant. In particular, we observe an outstanding error peak for $\omega = 2000$ for all polynomial order. We understand this experiment as an indication that the condition $\omega^{2p+1}h^{2p} \leq C$ might not be sufficient to guarantee a constant error independently of the frequency when the medium is heterogeneous.

Experiment 4				
p	n	ndf	m	err
1	10000	10001	10	4.67e-02
2	1200	3601	100	5.40e-02
3	610	3051	100	5.17e-02
4	375	2626	300	4.00e-02
5	275	2476	1000	4.61e-02
6	220	2421	1000	4.77e-02

Experiment 5				
p	n	ndf	m	err
1	5500	5501	1	4.01e-02
2	1000	3001	1	4.95e-02
3	550	2751	50	3.25e-02
4	370	2591	100	4.00e-02
5	285	2566	100	4.33e-02
6	270	2971	300	4.80e-02

Experiment 6				
p	n	ndf	m	err
1	25000	25001	100	4.58e-02
2	3000	9001	200	2.83e-02
3	1700	8501	300	2.45e-02
4	1150	8051	300	2.18e-02
5	900	8101	1000	5.25e-02
6	700	7701	1000	5.32e-02

TABLE 5. Comparison of different order of discretization for $\omega = 500$

6.5. **Experiments 4, 5 and 6.** In Experiment 4, we observed that the condition $\omega^{2p+1}h^{2p} \leq C$ is not satisfactory. Though we do not reproduce the tables here, we observe the same behaviour in Experiment 5 and 6.

We are not able to give a clear interpretation of difference between Experiments one to three and four to six, a part saying that the optimal homogeneous meshing condition does not seem to be enough for rough velocity parameters.

Though the meshing condition is not satisfactory, we are still able to show the advantage of higher order methods. To this end, we consider the problem of obtaining a relative error of 5% for a given frequency of $\omega = 500$. Table 5 shows that for higher discretization orders, the finite element linear system is smaller. More precisely, the best choice is $p = 6$ in Experiments 4 and 6 and $p = 5$ in Experiment 5.

7. 2D NUMERICAL EXPERIMENTS

In this section, we consider a more realistic example. We discretize the Helmholtz equation in a 2D medium $\Omega = (0,1)^2$ and search for $u \in H^1(\Omega)$ such that

$$\begin{cases} -\dfrac{\omega^2}{c^2} - \Delta u &= \delta_{x_c} \quad \text{in } \Omega, \\ u &= 0 \quad \text{on } \Gamma_D, \\ \nabla u \cdot n_\Omega - \dfrac{\mathbf{i}\omega}{c} u &= 0 \quad \text{on } \Gamma_A, \end{cases}$$

where $\Gamma_D = (0,1) \times \{0\}$ and $\Gamma_A = \partial\Omega \setminus \Gamma_D$. The right hand side is the Dirac mass $\delta_{x_c} \in H^1(\Omega)'$ centered at $x_c = (0.5, 0.1)$:

$$\langle \delta_{x_c}, \phi \rangle = \overline{\phi(x_c)} \quad \forall \phi \in H^1(\Omega).$$

The wavespeed $c \in L^\infty(\Omega)$ is depicted on Figure 2. Like in the one-dimensional experiments, we consider values ranging from 1 to 6, which is consistent with geophysical applications. Furthermore, Γ_D represents the surface of the Earth and the Dirichlet boundary condition corresponds to a free-surface condition. On the other hand, the boundary Γ_A is artificially build to bound the computational domain and an absorbing boundary condition is used to simulate a semi-infinite propagation medium.

Since no analytical solution is available for this benchmark, we consider a finite-element solution u_{ref} computed on a fine fitting mesh as a reference. Then, every computed numerical solution u_{num} is evaluated on a fixed 1000×1000 cartesian grid. As a result, we compute the relative L^2 error of numerical solutions with

$$E = \sqrt{\frac{\sum_{i,j=1}^{1000} |u_{num}(x_i, z_j) - u_{ref}(x_i, z_j)|^2}{\sum_{i,j=1}^{1000} |u_{ref}(x_i, z_j)|^2}},$$

where x_i and z_j correspond to the grid nodes.

Because we are targeting inverse problems in Geophysics as application, we consider frequencies f ranging from 5 to 20 Hz, the angular frequency being defined as $\omega = 2\pi f$.

We use classical C^0 Lagrangian finite elements based on triangular meshes. In order to fully take advantage of high order polynomials, we carry out static condensation to remove the internal degrees of freedom of each cell. Hence, the number of degrees of freedom indicated corresponds to the number of degrees of freedom after static condenstion, i.e. without the internal degrees of freedom.

We start by computing numerical solutions on a fitting mesh, i.e. a mesh so that c is constant inside each cell K. With such a mesh, we compute accurate solutions with the standard finite element method. However, the mesh size h is limited by the size of the layers of c in this case. The aim of this experiment is then to show the interest of using non-fitting meshes with larger cells. Indeed, our examples demonstrate that if the MMAm is used, accurate solutions can be computed on coarser meshes at a lower computational cost.

The fitting mesh is generated with the software `triangle` [10]. More precisely, we use the command

```
$ triangle -PAne -q33. geometry.poly
```

which mean that we ask `triangle` to exactly mesh the geometry, with a minimal angle condition of 33 degrees. Thus, we can expect that our fitting mesh is nearly optimal in the sense that it is close to be the coarsest mesh which fits the geometry with this minimal angle condition. The fitting mesh is depicted at Figure 3. It is made of $n = 10799$ triangular cells.

On the other hand, the MMAm can naturally handle non-fitting meshes. Thus, we use simple meshes based on cartesian grids for the MMAm as depicted on Figure 3. It is worth pointing out that since these meshes do not need to fit the wavespeed, we can select larger mesh steps h than the fitting mesh. As shown in Table 6, this is highlighted by the fact that the number of cells n used in the MMAm simulations is always less than 10799.

We use $m = 1024$ subcells for the quadrature subscheme in every MMAm experiments.

Table 6 presents the relative L^2 errors measured for each experiment. For each frequency, the first line of the table corresponds to the FEm solution computed with the fitting mesh. The other lines correspond to MMAm solutions computed with non-fitting meshes. Broadly speaking, Table 6 shows that the MMAm is able to achieve more than 5% accuracy even with non-fitting meshes. Also, especially for the lowest frequencies, the MMAm makes it

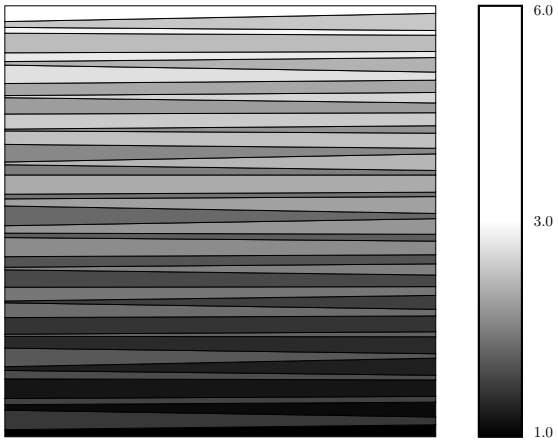

FIGURE 2. Wavespeed used in the 2D experiment

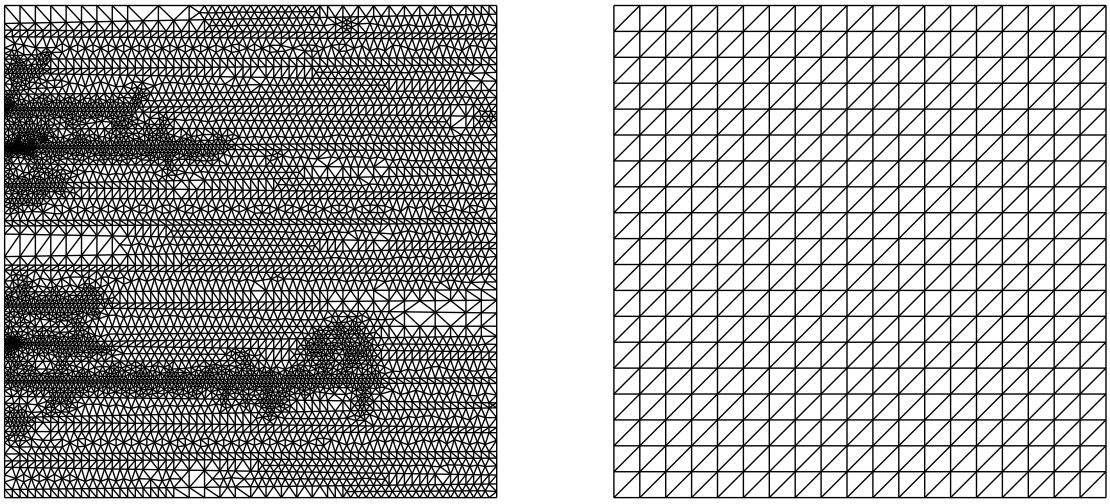

FIGURE 3. Fitting (left) and non-fitting (right) meshes

possible to drastically reduce the number of mesh cells n, at the price of increasing the order of discretization p.

In order to analyse more precisely the advantage of using a non-fitting mesh with the MMAm, we refer the reader to Table 7. In there, we compare the number of degrees of freedom required to achieve a comparable level of accuracy with the standard FEm, and the MMAm. From the first two rows of Table 7, we see that for the frequencies $f = 5$ and 10 Hz, the MMAm requires 8 times less degrees of freedom than the standard FEm.

	$f = 5$ Hz					
n	p=1	p=2	p=3	p=4	p=5	p=6
10799	13.3	3.85	2.11	1.19	0.697	0
3042	21.3	4.76	3.78	2.39	1.99	1.53
2312	19.5	5.47	2.67	2.07	1.27	0.998
1682	28.1	7.46	4.85	3.50	2.82	2.14
1152	29.6	8.57	4.39	2.73	2.31	1.63
722	42.3	11.7	7.36	5.33	4.51	3.52
392	50.6	13.5	9.71	5.60	3.61	2.92
162	79.7	26.9	13.8	11.1	8.57	7.24
32	149	74.5	42.5	23.8	15.3	14.0

	$f = 10$ Hz					
n	p=1	p=2	p=3	p=4	p=5	p=6
10799	37.9	3.61	1.50	0.836	0.489	0
3042	63.4	4.61	2.90	1.82	1.51	1.21
2312	69.3	6.26	2.19	1.65	1.12	0.987
1682	82.9	10.5	4.37	2.86	2.24	1.83
1152	97.6	15.5	4.40	2.56	2.34	1.92
722	105	29.6	7.57	5.39	3.90	2.99
392	117	42.9	14.4	5.47	4.05	3.62
162	104	92.8	38.4	14.8	10.4	8.31
32	153	115	131	98.1	87.8	34.9

	$f = 15$ Hz					
n	p=1	p=2	p=3	p=4	p=5	p=6
10799	136	13.7	1.01	0.457	0.263	0
3042	127	27.2	5.45	1.87	1.62	1.53
2312	122	44.9	12.9	3.24	2.63	2.36
1682	112	67.6	18.6	4.94	3.85	3.56
1152	104	102	30.0	12.7	5.55	5.11
722	105	136	39.5	22.2	8.91	6.74
392	101	128	75.6	30.8	18.4	11.0
162	101	104	122	98.2	52.3	33.4
32	99.9	101	99.3	111	122	122

	$f = 20$ Hz					
n	p=1	p=2	p=3	p=4	p=5	p=6
10799	114	60.5	5.61	0.746	0.375	0
3042	113	97.3	20.8	4.78	3.64	3.43
2312	116	109	38.9	7.70	4.21	3.75
1682	113	107	59.1	17.9	6.78	4.50
1152	110	111	86.4	38.7	14.2	7.83
722	102	111	109	69.2	30.7	14.3
392	101	124	113	109	67.8	39.0
162	101	101	115	101	101	85.6
32	100	106	102	103	108	135

TABLE 6. Relative L^2 error for the 2D experiment

	FEm				MMAm			
f	n	p	ndf	err	n	p	ndf	err
5 Hz	10799	2	21.852	3.85	392	5	2.689	3.61
10 Hz	10799	2	21.852	3.61	392	5	2.689	4.05
15 Hz	10799	3	38.177	1.01	3042	4	15.523	1.87
20 Hz	10799	3	38.177	5.61	1682	6	13.805	4.50

TABLE 7. Standard FEm versus MMAm

Furthermore, the last two lines indicate that the MMAm requires 2 times less degrees of freedom for the frequencies $f = 15$ and 20 Hz.

Since the fitting mesh is considered to be close to optimal, we do not think it is possible to reduce the computational cost of the standard FEm. Indeed, it is not possible to increase the mesh step of the fitting mesh in such way that the coarsened mesh still fits the wavespeed.

Therefore, this benchmark strongly hightlights the advantage of the MMAm over standard FEm. Indeed, the ability to use non-fitting meshes slightly reduces the computational cost for equivalent levels of accuracy.

Conclusion

In this work, we have applied the MMAm to the simplest one dimensional heterogeneous Helmholtz problem. We have focused on the superiority of high order polynomial discretizations over low order to solve this problem. Our other goal was to understand whether or not the optimal pre-asymptotic error estimate of [5, 6] is valid in heterogeneous media.

We have started with a detailed analysis of the continuous Helmholtz problem together with its MMAm discretization. We were able to show asymptotic error estimates up to $p = 3$ and recover the results demonstrated in [8, 9] for the homogeneous case. Even though those results are asymptotic and do not cover practical applications for meshing condition, we believe they are interesting because they show that $p = 3$ output performs $p = 1$ discretization at high frequencies even if the solution is only H^2 (our non-optimal $p = 3$ meshing condition is less restrictive than the optimal $p = 1$ condition of [5]). This result is an extension of the ideas of [8] where it is shown than the oscillatory character of the solution is regular, so that the pollution effect is reduced by high order methods even if the solution is not smooth.

One-dimensional numerical experiments validate our main results: the number of required degrees of freedom for a given accuracy is generally less for higher order discretizations even on non-fitting meshes with rough velocity contrasts. However, our experiments also show that the situation of heterogeneous media is truly more complex than homogeneous media. Indeed, in our examples, the pre-asymptotic meshing condition of homogeneous media do not seem enough to guarantee a constant error on the numerical solution when the medium is highly heterogeneous.

We have also considered a two-dimensional numerical experiment designed to be representative of geophysical applications. For this benchmark, the MMAm requires from 2 to 8 times less degrees of freedom than the standard FEm for an equivalent accuracy level.

We conclude that high order methods outperform linear discretizations assuming that the medium is properly approximated through a multiscale strategy. The MMAm is equivalent to the use of a velocity-adapted quadrature scheme and can be seen as a simple, local preprocessing stage for assembling the finite element linear system. In particular, this stage is highly parallelisable, requires a constant amount of memory and the resulting linear system has the exact same shape as the usual finite element system where the velocity is assumed to be constant in each cell.

We believe that our theoretical results together with the numerical experiments assert that the MMAm coupled with high order polynomials is a superior alternative to classical finite element discretizations.

APPENDIX

Proposition 6. *For all $u \in H^1(0,Z)$, there holds*

$$-2Re \int_0^Z \frac{1}{c^2} uz\bar{u}' = \int_0^Z \frac{1}{c^2}|u|^2 + \sum_{l=1}^{L-1} \left[\frac{1}{c^2}\right]_l z_l |u(z_l)|^2 - \frac{Z|u(Z)|^2}{c_{min}^2}. \tag{39}$$

Proof. As a starting point, we divide the integral onto the region where c is constant, and integrate by part.

$$\begin{aligned}
2\mathrm{Re} \int_0^Z \frac{1}{c^2} uz\bar{u}' &= \int_0^Z \frac{1}{c^2} z\,(2\mathrm{Re}\ u\bar{u}') \\
&= \int_0^Z \frac{1}{c^2} z \frac{d}{dz}|u|^2 \\
&= \sum_{l=1}^{L} \frac{1}{c_l^2} \int_{z_{l-1}}^{z_l} z\frac{d}{dz}|u|^2 \\
&= \sum_{l=1}^{L} \frac{1}{c_l^2} \left\{ -\int_{z_{l-1}}^{z_l} |u|^2 + \left[z|u|^2\right]_{z_{l-1}}^{z_l} \right\} \\
&= -\int_0^Z \frac{1}{c^2}|u|^2 + \sum_{l=1}^{L} \frac{1}{c_l^2} \left[z|u|^2\right]_{z_{l-1}}^{z_l}
\end{aligned}$$

To conclude, observe that the last term can be expended as

$$\begin{aligned}
\sum_{l=1}^{L} \frac{1}{c_l^2} \left[z|u|^2\right]_{z_{l-1}}^{z_l} &= \frac{Z|u(Z)|^2}{c_{min}^2} + \sum_{l=1}^{L-1} \left(\frac{1}{c_l^2} - \frac{1}{c_{l+1}^2}\right) z_l |u(z_l)|^2 \\
&= \frac{Z|u(Z)|^2}{c_{min}^2} - \sum_{l=1}^{L} \left[\frac{1}{c^2}\right]_l z_l |u(z_l)|^2.
\end{aligned}$$

□

Proposition 7. *For all $u \in H^2(0,Z)$, there holds*

$$2Re \int_0^Z u'(z\bar{u}')' = \int_0^Z |u'|^2 + Z|u'(Z)|^2. \tag{40}$$

Proof. First, we develop $(z\bar{u}')' = z\bar{u}'' + \bar{u}'$. Then since

$$2\mathrm{Re} \int_0^Z u' z\bar{u}'' = \int_0^Z z(2\mathrm{Re}\ u'\bar{u}'') = \int_0^Z z\frac{d}{dz}|u'|^2 = -\int_0^Z |u'|^2 + [z|u'|^2]_0^Z,$$

the result follow. □

References

[1] H. Barucq, T. Chaumont-Frelet, and C. Gout. Stability analysis of heterogeneous helmholtz problems and finite element solution based on propagation media approximation. *submitted*, 2014.

[2] N. Collier, D. Pardo, L. Dalcin, M. Paszynski, and V.M. Calo. The cost of continuity: A study of the performance of isogeometric finite elements using direct solvers. *Computer Methods in Applied Mechanics and Engineering*, 213-216:353–361, 2012.

[3] J. Douglas, J.E. Santos, D. Sheen, and L. Bennethum. Frequency domain treatment of one-dimensional scalar waves. *Mathematical Models and Methods in Applied Sciences*, 3(2):171–194, 1993.

[4] U. Hetmaniuk. Stability estimates for a class of helmholtz problems. *COMMUN. MATH. SCI.*, 2007.

[5] F. Ihlenburg and I. Babuška. Finite element solution of the helmholtz equation with high wave number part i: The h-version of the fem. *Computers Math. Applic.*, 30(9):9–37, 1995.

[6] F. Ihlenburg and I. Babuška. Finite element solution of the helmholtz equation with high wave number part ii: The h-p version of the fem. *SIAM J. Numer. Anal.*, 34(1):315–358, 1997.

[7] J.M. Melenk. *On generalized finite element methods*. PhD thesis, University of Maryland, 1995.

[8] J.M. Melenk and S.A. Sauter. Convergence analysis for finite element discreizations of the helmholtz equation with dirichlet-to-neumann boundary conditions. *Math. Comp.*, 79:1871–1914, 2010.

[9] J.M. Melenk and S.A. Sauter. Wavenumber explicit convergence analysis for galerkin discretizations of the helmholtz equation. *SIAM J. Numer. Anal.*, 49(3):1210–1243, 2011.

[10] J.R. Shewchuk. Triangle: Engineering a 2D Quality Mesh Generator and Delaunay Triangulator. In Ming C. Lin and Dinesh Manocha, editors, *Applied Computational Geometry: Towards Geometric Engineering*, volume 1148 of *Lecture Notes in Computer Science*, pages 203–222. Springer-Verlag, May 1996. From the First ACM Workshop on Applied Computational Geometry.

[11] I. Babuška and S. Sauter. Is the pollution effect of the fem avoidale for the helmholtz equation considering high wave numbers? *SIAM REVIEW*, 42(3):451–484, 2000.

(T. Chaumont-Frelet) INRIA Research Centre Bordeaux Sud-Ouest IPRA, University of Pau, IPRA, BP 1155, 64013 Pau, France and Normandie Université, INSA de Rouen, LMI, Av. de l'Université, 76801 St Etienne du Rouvray cedex, France

Current address: Basque Center for Applied Mathematics, Alameda Mazarredo, 14, 48009 Bilbao, Bizkaia, Spain

E-mail address: theophile.chaumont_frelet@insa-rouen.fr